ETH
Eidgenössische Technische Hochschule Zürich
Swiss Federal Institute of Technology Zurich

Institut für Integrierte Systeme
Integrated Systems Laboratory

DEPARTMENT OF
INFORMATION TECHNOLOGY AND ELECTRICAL ENGINEERING

Fall Semester 2025

Comprehensive Evaluation of Sparse Symmetric Matrix Permutation Methods

Master Thesis

Ritvik Ranjan
rranjan@ethz.ch

October 4, 2025

Advisors: Vincent Maillou, vmaillou@iis.ee.ethz.ch
Dr. Alexandros Nikolaos Ziogas, alziogas@iis.ee.ethz.ch

Professor: Prof. Dr. Mathieu Luisier, leader@iis.ee.ethz.ch

Abstract

Sparse symmetric linear systems arise across computational science and engineering. Solving these systems efficiently via direct methods depends critically on matrix reordering to minimize fill-in during factorization. Finding optimal reorderings is NP-complete, necessitating good heuristic approaches. This thesis presents a comprehensive evaluation of sparse matrix reordering algorithms, comparing classical methods, graph partitioning approaches, and hypergraph-based techniques across diverse matrix structures. We assess multiple performance metrics including fill-in reduction, execution time, memory usage, and parallelization potential. Our benchmarking reveals that advanced methods achieve better fill-in reduction compared to classical algorithms, though at higher computational cost. We implemented a few enhancements, including a Nested Dissection variant with improved coarsening and a GPU-accelerated RCM implementation, demonstrating significant performance improvements. The results establish some trade-offs between ordering quality and computational overhead, providing guidance for algorithm selection and future research directions in sparse matrix reordering.

On the cover: Reorderings and the original graph of the Jazz musicians (1912-1940) collaboration network.

Acknowledgments

First and foremost, I would like to thank Prof. Dr. Mathieu Luisier for providing me with the opportunity to work in the Nano-TCAD group and on this fascinating topic.

I would like to thank Vincent Maillou for providing me the opportunity to work on this project and for his friendly and helpful supervision and the patience and time put into teaching me different aspects of it. I express my sincere thanks to Dr. Alexandros Nikolaos Ziogas for being supportive and guiding me through the process.

Eidgenössische Technische Hochschule Zürich
Swiss Federal Institute of Technology Zurich

Declaration of originality

The signed declaration of originality is a component of every written paper or thesis authored during the course of studies. **In consultation with the supervisor**, one of the following two options must be selected:

☐ I hereby declare that I authored the work in question independently, i.e. that no one helped me to author it. Suggestions from the supervisor regarding language and content are excepted. I used no generative artificial intelligence technologies[1].

☒ I hereby declare that I authored the work in question independently. In doing so I only used the authorised aids, which included suggestions from the supervisor regarding language and content and generative artificial intelligence technologies. The use of the latter and the respective source declarations proceeded in consultation with the supervisor.

Title of paper or thesis:

Comprehensive Evaluation of Sparse Symmetric Matrix Permutation Methods

Authored by:
If the work was compiled in a group, the names of all authors are required.

Last name(s):	**First name(s):**
Ranjan	Ritvik

With my signature I confirm the following:
- I have adhered to the rules set out in the Citation Guidelines.
- I have documented all methods, data and processes truthfully and fully.
- I have mentioned all persons who were significant facilitators of the work.

I am aware that the work may be screened electronically for originality.

Place, date	**Signature(s)**
Zürich, 06.10.25	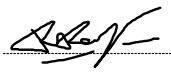
	If the work was compiled in a group, the names of all authors are required. Through their signatures they vouch jointly for the entire content of the written work.

[1] For further information please consult the ETH Zurich websites, e.g. https://ethz.ch/en/the-eth-zurich/education/ai-in-education.html and https://library.ethz.ch/en/researching-and-publishing/scientific-writing-at-eth-zurich.html (subject to change).

Contents

Chapter 1

Introduction

Sparse linear systems of the form $Ax = b$, where $A \in \mathbb{R}^{n \times n}$ is sparse and symmetric positive definite, are ubiquitous in modern scientific computing. These systems arise naturally across virtually every domain of computational science and engineering, including quantum chemistry, computer graphics, computational fluid dynamics, power networks, machine learning, and optimization. Formally, one may state matrix A is considered sparse when the number of nonzero entries $\text{nnz}(A)$ satisfies $\text{nnz}(A) = O(n)$ rather than $O(n^2)$ as in dense matrices, although a better practical definition is a matrix is sparse if it is advantageous to exploit its zero entries [1].

This sparsity typically arises from the discretization of partial differential equations (PDEs)[2] using finite difference, finite element, or finite volume methods. When continuous problems described by partial differential equations are discretized using methods such as finite differences, finite elements, or finite volumes, the resulting algebraic equations connect only neighboring (or some specific) grid points or elements. Conceptually, sparsity corresponds to systems with few pairwise interactions. For instance, in a three-dimensional finite element mesh, each node typically connects to only a small neighborhood of adjacent nodes, regardless of the total problem size, resulting in matrices where the number of non-zero elements is roughly equal to the number of rows or columns rather than being proportional to n^2.

As we see in Fig. 1.1, the Cholesky factorization of a sparse matrix often results in a denser matrix due to fill-in, where zero entries in the original matrix become non-zero in the factorized form. This fill-in can significantly increase both memory usage and computational time for solving the system. The amount of fill-in depends on the order in which variables are eliminated during factorization, which is determined by the ordering, or permutation, of the matrix rows and columns. The permutations serve as a preprocessing step that can reduce fill-in largely. The basic principle involves reordering the rows and columns of the matrix A to obtain a permuted system $PAP^T\hat{x} = Pb$, where P is a permutation matrix, such that the reordered matrix exhibits superior properties for factorization.

In this thesis, we focus exclusively on the permutation problem for sparse symmetric

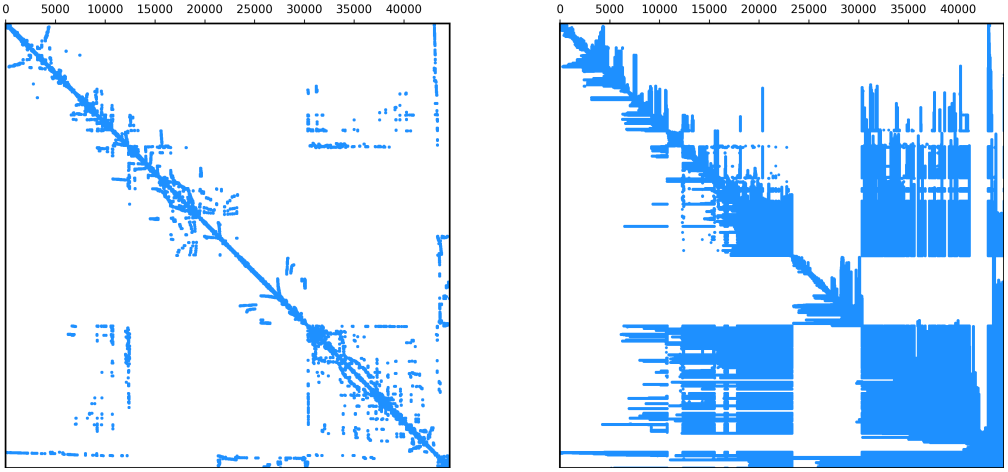

Figure 1.1.: Sparsity pattern of a matrix from structural engineering `bcsstk32` (left) and $L + L^T$ (right) where L is the Cholesky factor of `bcsstk32`.

matrices. We explore existing methods for sparse symmetric matrix reordering, investigate potential optimizations and parallelization strategies, and evaluate the performance of different reordering methods across a variety of matrices, assessing their effectiveness in terms of fill-in reduction, memory usage and parallelism. In chapter 2, we provide the necessary theoretical background on sparse matrix factorization and graph representations. Chapter 3 details the implementation of various reordering algorithms, while chapter 4 presents an overview of our experimental evaluation. For full performance results, please refer to the appendix A.

Chapter 2

Background

Before we look into the algorithms and theory behind reordering techniques, we first take a dive into the factorization process that produces further non-zeroes, which in this and the entire thesis's context, are called fill-in. It may be trivial but important to note, that if some numerical arithmetic results in a zero in the factored matrix, it is usually still considered as a fill-in.

Suppose the set of set of n equations that are to be solved are

$$Ax = b \tag{2.1}$$

where A is a sparse matrix, x is the vector of unknowns. The sparsity, or the number of non-zero entries in A determines the fill-in of it's Cholesky factor when it is employed to solve the aforementioned set of equations. Suppose the Cholesky factorization of A is given by LL^T, where L is a lower triangular matrix (with a positive diagonal) and L^T is the transpose of L. The efficiency of solving this set of equations is dependent on the number of non-zero entries in L. It has been shown that we can factor and solve the set of equations in space proportional to $\sum_j dj$ and time complexity $\sum_j {d_j}^2$, where d_j is the number of non-zeroes in the jth column of L [3].

2.1. Elimination Trees and Symbolic Factorization

2.1.1. Mathematical Foundations and Problem Formulation

Consider a sparse symmetric positive definite matrix $A \in \mathbb{R}^{n \times n}$. The Cholesky factorization decomposes A into the form $A = LL^T$, where L is a lower triangular matrix. While A may contain relatively few nonzero entries, the factor L typically exhibits significantly more nonzeros due to a phenomenon known as fill-in. This fill-in occurs because the elimination process creates new nonzero entries at positions that were originally zero in A.

The sparsity pattern of A is defined as the set $\text{pattern}(A) = \{(i,j) : A_{ij} \neq 0\}$. Similarly, $\text{pattern}(L)$ denotes the sparsity pattern of the Cholesky factor. The fundamental

observation is that pattern(L) can be completely determined from pattern(A) using purely structural analysis, without requiring any numerical computation. This structural predictability forms the theoretical foundation for elimination trees and symbolic factorization.

Every sparse symmetric matrix A can be naturally represented as an undirected graph $G(A) = (V, E)$, where the vertex set $V = \{1, 2, \ldots, n\}$ corresponds to the rows and columns of A, and the edge set E contains an edge (i, j) if and only if $A_{ij} \neq 0$ for $i \neq j$. This graph representation transforms matrix operations into graph-theoretic problems, enabling the application of powerful combinatorial methods to numerical linear algebra.

The elimination process on matrix A corresponds to a sequence of vertex eliminations on graph $G(A)$. When vertex k is eliminated, all pairs of neighbors of k become connected by edges if they were not already connected. This edge addition process continues throughout the elimination sequence, producing what is known as the filled graph $G^+(A)$. The filled graph contains all edges that exist at any point during the elimination process, and its structure completely determines the sparsity pattern of the Cholesky factor L.

The elimination tree provides a compact representation of the structural relationships inherent in sparse matrix factorization. This tree structure captures the essential dependencies between different stages of the elimination process.

Definition 2.1 (Elimination Tree)**.** Let A be a symmetric positive definite matrix with Cholesky factorization $A = LL^T$. The elimination tree $T(A) = (V, E_T)$ is a directed tree defined by the parent function parent : $V \to V \cup \{\emptyset\}$, where:

$$\text{parent}(j) = \min\{i > j : L_{ij} \neq 0\} \tag{2.2}$$

If no such index i exists, then parent$(j) = \emptyset$ and j is a root of the tree. The directed edges of the tree are given by $E_T = \{(j, \text{parent}(j)) : \text{parent}(j) \neq \emptyset\}$.

This definition establishes a precise correspondence between the numerical structure of the Cholesky factor and the combinatorial structure of a directed tree. Each node j in the tree corresponds to column j of the matrix, and the parent relationship encodes which column will first modify column j during the factorization process.

Definition 2.2 (Ancestor Relationship)**.** In the elimination tree $T(A)$, node i is an ancestor of node j (denoted $i \succ j$) if there exists a directed path from j to i in the tree. Node i is a proper ancestor if $i \succ j$ and $i \neq j$.

The ancestor relationship in the elimination tree has a profound connection to the structure of the Cholesky factor, as formalized in the following fundamental theorem.

Theorem 2.1 (Fundamental Characterization Theorem)**.** *Let $T(A)$ be the elimination tree of symmetric positive definite matrix A with Cholesky factor L. Then for any indices $i > j$: $L_{ij} \neq 0$ if and only if $i \succ j$ in $T(A)$.*

This theorem establishes that the elimination tree completely characterizes the sparsity pattern of the Cholesky factor. The nonzero entries in column j of L correspond exactly to

the ancestors of node j in the elimination tree. This remarkable result shows that purely combinatorial information (tree ancestry) determines numerical structural properties (matrix sparsity patterns).

2.1.2. Structural Properties and Theoretical Characterizations

Fill-in Characterization Through Path Analysis

Understanding when fill-in occurs during elimination requires analyzing connectivity patterns in the original matrix graph. The concept of fill paths provides a precise characterization of this phenomenon.

Definition 2.3 (Fill Path)**.** Let $G(A) = (V, E)$ be the graph of matrix A. A fill path from vertex i to vertex j (where $i < j$) is a path $P = (i = v_0, v_1, v_2, \ldots, v_k = j)$ in $G(A)$ such that all intermediate vertices satisfy $v_l < \min(i, j)$ for $1 \leq l \leq k - 1$.

The fill path condition ensures that all intermediate vertices on the path are eliminated before either endpoint, which is precisely the condition under which the elimination process will create a direct connection between i and j.

Theorem 2.2 (Fill Path Characterization)**.** *An edge (i, j) with $i < j$ belongs to the filled graph $G^+(A)$ if and only if there exists a fill path from i to j in the original graph $G(A)$.*

This theorem provides the theoretical foundation for predicting fill-in patterns. It shows that structural properties of the original graph completely determine which new edges will be created during elimination, independent of the specific numerical values in the matrix.

The elimination tree possesses several important structural properties that make it amenable to efficient algorithmic manipulation.

Theorem 2.3 (Postorder Property)**.** *In any elimination tree $T(A)$, if $\text{parent}(j) = i$, then all nodes in the subtree rooted at j have indices less than i. Furthermore, the elimination tree is uniquely determined by the sparsity pattern of A, independent of the specific elimination ordering used (provided the ordering respects the natural ordering of indices).*

This property implies that elimination trees can be processed using postorder traversal, where children are visited before their parents. This traversal order naturally reflects the dependencies in the elimination process—a column can only be processed after all columns in its subtree have been completed.

2.1.3. Algorithmic Construction of Elimination Trees

The most straightforward approach to constructing elimination trees directly implements the definition by examining the sparsity structure of the matrix.

This algorithm requires $O(|A|)$ time, where $|A|$ denotes the number of nonzero entries in matrix A. The space complexity is $O(n)$ for storing the parent array. While simple

Algorithm 1: Direct Construction Method

Input : Symmetric positive definite matrix A with sparsity pattern
Output: Parent array representing elimination tree $T(A)$

```
1  Initialize parent[1...n] ← 0 ;                    // 0 represents null parent
2  for j = 1 to n do
3  |   parent[j] ← 0;
4  |   foreach i ∈ {k : A[j,k] ≠ 0 and k > j} do
5  |   |   if parent[j] = 0 or i < parent[j] then
6  |   |   |   parent[j] ← i;
7  |   |   end
8  |   end
9  end
10 return parent array
```

to understand and implement, this direct approach does not exploit the structural properties of elimination trees for potential efficiency improvements.

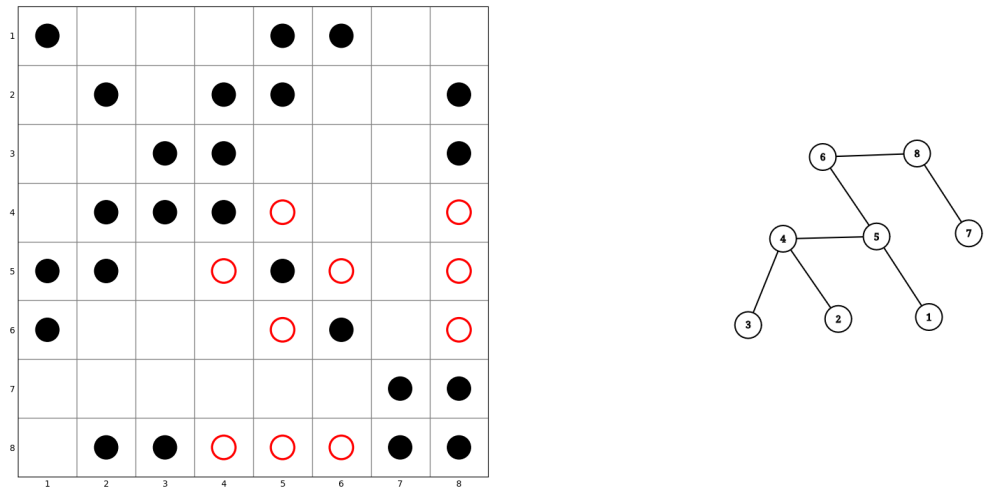

(a) Sparse matrix structure

(b) Corresponding elimination tree

Figure 2.1.: Illustration of elimination tree construction for the given sparse symmetric matrix. The sparsity is denoted by filled black circles and the fill-in induced is denoted by hollow red circles.

2.1.4. Symbolic Factorization

Symbolic factorization determines the sparsity pattern of the Cholesky factor L from the sparsity pattern of matrix A using the elimination tree. It does not involve any numerical

computations and relies solely on the structure of the original matrix.

The key insight is that the sparsity structure of each column in L can be computed by analyzing how structural information propagates through the elimination tree. Each column inherits structure from two sources: the original matrix A and the previously computed columns corresponding to its children in the elimination tree.

Definition 2.4 (Column Structure Inheritance)**.** For column j of the Cholesky factor L, the nonzero pattern is determined by:

- Direct inheritance: All nonzero entries from column j of the original matrix A that lie on or below the diagonal
- Indirect inheritance: All entries from the union of nonzero patterns of columns corresponding to children of j in the elimination tree, restricted to rows numbered greater than j

This inheritance pattern reflects the computational dependencies during numerical factorization—column j can only be processed after all its children in the elimination tree have been completed.

Algorithm 2: Elimination Tree Symbolic Factorization

Input : Sparsity pattern of matrix A, elimination tree $T(A)$
Output: Sparsity pattern of Cholesky factor L

Initialize column_structure$[1 \dots n]$ as empty sets;
for $j = 1$ **to** n ; `// in postorder traversal of` $T(A)$
do
  `// Direct inheritance from original matrix`
  column_structure$[j] \leftarrow \{i \geq j : A[i,j] \neq 0\}$;
  `// Indirect inheritance from children in elimination tree`
  foreach *child c of j in* $T(A)$ **do**
    column_structure$[j] \leftarrow$ column_structure$[j] \cup \{i \in$ column_structure$[c] : i > j\}$;
  end
  `// Record structure for column` j `of` L
  pattern$(L[:,j]) \leftarrow$ column_structure$[j]$;
end
return *pattern*(L)

The postorder traversal ensures that each column is processed only after all its descendants in the elimination tree have been completed, respecting the computational dependencies inherent in the factorization process.

2.2. Minimum fill-in and NP-completeness

When performing Cholesky factorization on a sparse symmetric matrix, we want to minimize fill-in - the new nonzero entries that appear during elimination. This translates to a graph theory problem: given a graph representing the matrix's sparsity pattern, find an elimination order that creates the fewest new edges. Yannakakis [4] proved that this optimization problem is NP-complete, meaning no polynomial-time algorithm can solve it optimally in general (unless P = NP).

The key insight connecting linear algebra to graph theory is that chordal graphs are essential in proving this. A graph is chordal if every cycle of length ≥ 4 has a chord (an edge connecting non-consecutive vertices). The fundamental theorem states that a graph has perfect elimination (zero fill-in) if and only if it is chordal, and any elimination process on any graph produces a chordal result. Therefore, the minimum fill-in problem becomes: What is the smallest number of edges we must add to make our graph chordal?

The proof uses a three-step reduction to prove NP-completeness. First, we consider bipartite graphs and their special case, chain graphs. A bipartite graph has vertices split into two independent sets P and Q, and it is a chain graph when neighborhoods form a nested sequence: $\Gamma(v_1) \subseteq \Gamma(v_2) \subseteq \ldots \subseteq \Gamma(v_k)$. The key property is that a bipartite graph is a chain graph if and only if it contains no pair of independent edges.

Second, for any bipartite graph $G = (P, Q, E)$, we construct $C(G)$ by making P into a complete clique (all vertices in P connected), making Q into a complete clique (all vertices in Q connected), and keeping original edges between P and Q. The crucial lemma states that $C(G)$ is chordal if and only if G is a chain graph. This works because if G has independent edges, they create a 4-cycle in $C(G)$ with no chord. Conversely, if G is a chain graph, $C(G)$ has a perfect elimination order.

Third, the reduction uses the Optimal Linear Arrangement Problem, which asks: given a graph, arrange vertices on a line to minimize the sum of distances between adjacent vertices. This problem is known to be NP-complete. Yannakakis constructs an transformation where, given graph G with n vertices and m edges, he creates bipartite graph G' where part P has one vertex for each vertex in G, and part Q has an elaborate gadget structure with $2m + n^2 - d(v)$ vertices, with connections that encode the linear arrangement constraints. The mathematical relationship is:

$$\text{Minimum fill-in of } G' = \text{Optimal arrangement cost of } G + \frac{n^2(n-1)}{2} - 2m \tag{2.3}$$

This result has practical implications that no perfect algorithm exists, as any algorithm guaranteeing optimal fill-in will require exponential time in the worst case. This explains why practical sparse matrix reordering uses heuristics like minimum degree ordering, nested dissection and such.

2.3. Heuristics classification

There are several heuristics that have been proposed to reduce the fill-in developed over the years. These heuristics can be broadly classified in the following categories:

Bandwidth minimization, minimum degree (and it's variants), nested dissection, banded structure methods using hypergraphs, and recently, machine learning approaches.

2.3.1. Bandwidth Minimization

Bandwidth minimization refers to the problem of permuting the rows and columns of a matrix such that the non-zero entries are as close to the diagonal as possible. Gaussian elimination can be performed in $O(nb^2)$ time on matrices of dimension n and bandwidth b, which is faster than the forward $O(n^3)$ algorithm when b is smaller than n (Lim A. et al., 2006a). Additionally, this problem is NP-complete, but several heuristics have been developed to approximate the optimal solution.

The Cuthill-McKee algorithm [5] employs breadth-first search to reduce matrix bandwidth by generating level structures. However, it has computational limitations and may not achieve optimal bandwidth reduction. The Reverse Cuthill-McKee algorithm [6] addresses these issues by reversing the ordering, while the GPS algorithm by Gibbs et al. provides an alternative level structure approach.

We take a look at the reverse Cuthill-McKee algorithm, which is still widely used in practice.

[write the pseudocode here]

2.3.2. Minimum Degree

The minimum degree algorithm [7] determines the order in which to eliminate variables (or pivot) during Gaussian elimination to minimize fill-in (creation of new non-zero entries) in sparse matrices. At each step, it chooses the node with the minimum degree (fewest connections) for elimination.

The minimum degree algorithm operates on the adjacency graph of the sparse matrix. It begins by initializing the graph, where each vertex represents a variable. At each iteration, the algorithm selects the vertex with the smallest degree (i.e., the fewest neighbors), which corresponds to the variable whose elimination is expected to introduce the least fill-in. Upon elimination, the chosen vertex is removed from the graph, and all its neighbors are connected to each other, forming a clique to preserve the matrix structure. The degrees of the affected vertices are then updated to reflect the new connections. This process is repeated until all vertices have been eliminated. The resulting elimination order directly determines the pivot sequence used during matrix factorization.

Variants of the minimum degree algorithm include:

1. Multiple Minimum Degree (MMD) [8]

   When multiple nodes have the same minimum degree, uses additional tie-breaking rules. Often selects based on secondary criteria like external degree or node numbering.

2. Approximate Minimum Degree (AMD) [9]

Uses approximations to avoid expensive exact degree calculations. Employs concepts like "supervariables" and "element absorption". Much faster than exact minimum degree while maintaining similar fill-in quality.

3. Constrained Minimum Degree

   Incorporates additional constraints (like maintaining bandwidth). Balances minimum degree objective with other structural requirements.

2.3.3. Nested Dissection

Nested dissection is a divide and conquer heuristic for the solution of sparse symmetric systems of linear equations based on graph partitioning. Nested dissection can be viewed as a recursive divide-and-conquer algorithm on an undirected graph; it uses separators in the graph, which are small sets of vertices whose removal divides the graph approximately in half [10].

(a) Original graph before separator identification

(b) Graph after separator removal showing partitioned subgraphs

Figure 2.2.: Separator identification process. The separator vertices divide the graph into approximately equal subgraphs

Nested dissection consists of the following steps: Form an undirected graph in which the vertices represent rows and columns of the system of linear equations, and an edge represents a nonzero entry in the sparse matrix representing the system. Recursively partition the graph into subgraphs using separators, small subsets of vertices the removal of which allows the graph to be partitioned into subgraphs with at most a constant fraction of the number of vertices. Perform Cholesky decomposition (a variant of Gaussian elimination for symmetric matrices), ordering the elimination of the variables by the recursive structure of the partition: each of the two subgraphs formed by removing the separator is eliminated first, and then the separator vertices are eliminated [11].

All the sequential algorithms for determining the elimination ordering of a graph G can be described by the following general algorithm: Generate the tree of separators for G and perform a tree traversal on the separator tree to order the vertices, where this traversal must visit a node before any of its parents.

2.3.4. Hypergraph partitioning and other methods

In recent years, hypergraph partitioning methods [12] have been proposed to reduce fill-in during sparse matrix factorization. Hypergraphs generalize graphs by allowing edges (hyperedges) to connect more than two vertices, making them well-suited for modeling complex relationships in sparse matrices. In this paper we explore another Hypergraph based reordering method,

Other methods include machine learning approaches that learn optimal ordering strategies using reinforcement learning. One such approach is Alpha Elimination [13] which uses Convolutional Neural Networks (CNNs) and reinforcement learning to predict the next node to eliminate based on the current state of the graph. We have explored a more flexible architecture but fails with scalability, which we discuss in Chapter 5.

Chapter 3

Implementation and Optimizations

This chapter describes both the existing state-of-the-art implementations that form the baseline for comparison (Sections 3.1 and 3.2), as well as the new algorithms and implementations developed in this thesis (Sections 3.3, 3.4, and 3.5).

3.1. SuiteSparse implementation of RCM and Minimum Degree

The Reverse Cuthill-McKee (RCM) algorithm in SuiteSparse provides bandwidth reduction for symmetric sparse matrices through a breadth-first search strategy combined with degree-based ordering heuristics. The implementation processes disconnected components separately and employs pseudo-peripheral vertex selection to minimize profile and bandwidth.

The SuiteSparse RCM implementation incorporates several refinements over the basic algorithm. The pseudo-peripheral vertex selection uses multiple BFS traversals to identify vertices that are approximately diametrically opposite, which typically results in better bandwidth reduction than arbitrary starting points. The degree-based sorting of neighbors during BFS traversal helps create a more systematic ordering that tends to group low-degree vertices together, further improving the resulting bandwidth.

The algorithm's effectiveness stems from its ability to produce orderings where vertices with similar connectivity patterns are placed close together in the permutation. This locality property translates directly into reduced bandwidth and improved cache performance during matrix operations, making RCM particularly valuable for iterative solvers and direct factorization methods that benefit from band structure preservation.

3.1.1. AMD Algorithm Overview

The Approximate Minimum Degree (AMD) algorithm implemented in SuiteSparse follows a refined elimination-based approach that balances computational efficiency with fill-in minimization. The algorithm operates on a quotient graph representation and

Algorithm 3: SuiteSparse RCM Algorithm

input : Symmetric matrix A ($n \times n$)
output: Permutation P for bandwidth reduction

Initialize:;
Compute degree$[i] = |\text{adj}(i)|$ for all vertices i;
Find connected components $R_1, R_2, \ldots, R_k$ using DFS;
Initialize visited$[i]$ = false for all i;
Set perm_index = 0;
Process each component:;
foreach *connected component* R_j **do**
    Find pseudo-peripheral start vertex:;
    start = `FindPseudoPeripheral`(R_j);
    `// Select vertex with minimum degree among maximum-distance vertices`
    Cuthill-McKee BFS traversal:;
    Initialize queue $Q = \{\text{start}\}$;
    Set visited[start] = true;
    Initialize CM_order = [start];
    while $Q \neq \emptyset$ **do**
        $u = \text{dequeue}(Q)$;
        neighbors = sort(unvisited_adj(u),by_degree_ascending);
        foreach $v \in$ *neighbors* **do**
            if $\neg$*visited*$[v]$ **then**
                Set visited$[v]$ = true;
                enqueue(Q, v);
                Append v to CM_order;
            end
        end
    end
    Apply reverse ordering (RCM):;
    for $i = 0$ **to** $|CM\_order| - 1$ **do**
        P[perm_index $+ i$] = CM_order[|CM_order| $- 1 - i$];
    end
    perm_index $\leftarrow$ perm_index $+$ |CM_order|;
end
return P;

incorporates several key optimizations including aggressive absorption, approximate degree updates, and dense row detection.

The key innovation in SuiteSparse's AMD implementation lies in its aggressive absorption strategy and approximate degree computation. The aggressive absorption phase identifies elements that can be completely absorbed into the current pivot, reducing the size of the quotient graph and improving cache locality. The approximate degree updates provide a computationally efficient method to maintain ordering decisions without exact degree computation, which becomes prohibitively expensive as elimination progresses.

The dense row detection mechanism addresses a common pathology in minimum degree algorithms where elimination of high-degree vertices can lead to excessive fill-in. When the algorithm detects that a newly formed element exceeds a threshold based on the matrix size, it defers elimination of the associated variables, effectively implementing a hybrid strategy that combines minimum degree with nested dissection principles.

3.2. Nested Dissection using METIS and SCOTCH

Nested dissection represents a divide-and-conquer approach to matrix ordering that recursively partitions the graph using small vertex separators, ordering the separated components before the separator vertices. METIS and SCOTCH implement sophisticated multilevel nested dissection algorithms that combine graph coarsening, separator finding, and refinement techniques to produce high-quality orderings for large sparse matrices.

The multilevel nested dissection approach in METIS provides superior ordering quality compared to single-level methods by operating at multiple scales. The coarsening phase creates a hierarchy of increasingly smaller graphs while preserving essential structural properties through heavy edge matching. This matching strategy prioritizes edges with large weights, which in the context of matrix ordering typically correspond to strong structural connections that should be preserved during coarsening.

The separator computation on the coarsest level benefits from reduced problem size while maintaining global structural awareness. The refinement phase during projection ensures that separators remain high-quality as they are mapped back to finer graph levels. The recursive application of this process creates a natural hierarchy where large components are isolated first, followed by progressively smaller substructures, resulting in elimination orderings with excellent fill-in characteristics for sparse direct solvers.

Algorithm 4: SuiteSparse AMD Algorithm

input : Symmetric matrix A ($n \times n$), Control parameters
output: Permutation P, Info statistics

Initialize:;
Convert A to $A + A^T$ pattern if unsymmetric;
Build quotient graph $G = (V, E)$ from A;
Initialize degree lists Head$[d]$ for $d = 0$ to n;
Set degree$[v] = |\text{adj}(v)|$ for all vertices v;
Place each vertex in appropriate degree list;
Main elimination loop:;
for $k = 1$ **to** n **do**
    Select pivot:;
    Find minimum degree d with non-empty Head$[d]$;
    Select pivot p from Head$[d]$;
    Remove p from degree list;
    Set $P[k] = p$ (add to elimination ordering);
    Element absorption:;
    foreach *element e adjacent to p* **do**
        if $|L_e \cap L_p| = |L_e|$ **then**
            Absorb e into p (aggressive absorption);
        end
    end
    Form new element e_p*:*;
    $L_{e_p} = \text{adj}(p) \setminus \{\text{absorbed elements}\}$;
    Mark e_p as new element;
    Update degrees (approximate):;
    foreach *uneliminated vertex* $v \in L_{e_p}$ **do**
        external_degree$[v] = |\text{adj}(v) \cap \text{uneliminated}|$;
        bound $= |L_{e_p}| - |L_{e_p} \cap \text{adj}(v)|$;
        degree$[v] \approx$ external_degree$[v]$ + bound;
        Move v to new degree list;
    end
    Dense row detection:;
    if $|L_{e_p}| > \max(\alpha\sqrt{n}, 16)$ **then**
        Mark e_p as dense element;
        Move dense variables to end of ordering;
    end
end
Post-processing:;
Apply elimination tree post-ordering;
Compute final permutation statistics;
return *P and Info*;

Algorithm 5: Multilevel Graph Coarsening

input : Graph $G = (V, E)$
output: Hierarchy of progressively coarser graphs

```
Hierarchy = [G] // Start with original graph
CurrentGraph = G;
while |V(CurrentGraph)| > COARSENING_THRESHOLD do
    Find heavy edge matching to preserve graph structure;
    Matching = HeavyEdgeMatching(CurrentGraph);
    Contract matched edges to create coarser graph;
    CoarserGraph = ContractEdges(CurrentGraph, Matching);
    Add to hierarchy;
    Hierarchy.append(CoarserGraph);
    CurrentGraph = CoarserGraph;
end
return Hierarchy;
```

Algorithm 6: Heavy Edge Matching Algorithm

input : Graph G with edge weights
output: Maximal matching favoring heavy edges

```
Matching = {};
Matched = {} // Track matched vertices
Sort edges by weight, centralness and degree for better matching quality;
SortedEdges = SortByWeight(E(G), descending = true);
foreach edge (u, v) in SortedEdges do
    if u ∉ Matched and v ∉ Matched then
        Matching.add((u, v));
        Matched.add(u);
        Matched.add(v);
    end
end
return Matching;
```

3.3. New Coarsening Approaches in Nested Dissection

This section presents a new coarsening algorithm developed in this thesis that improves upon the standard METIS approach.

The standard METIS coarsening approach uses heavy edge matching (SHEM) to create progressively smaller graphs while preserving structural properties. This work introduces a separator-aware heavy edge matching (SAHEM) algorithm that modifies the coarsening phase to better preserve separator structure during the multilevel nested

dissection process.

The SAHEM algorithm extends the standard heavy edge matching by incorporating separator likelihood scores for each vertex. These scores are computed using two local structural features: normalized degree centrality and local clustering coefficient. High-degree vertices with low clustering coefficients are more likely to be separators in the graph, as they connect different regions without being part of densely connected communities.

For each vertex, the algorithm computes a separator score as:

$$\text{sep\_score}(v) = \frac{\text{degree}(v)}{n} \times (1 - \text{clustering}(v))$$

The local clustering coefficient measures the fraction of possible edges that exist between a vertex's neighbors. Vertices with many neighbors but few connections among those neighbors typically serve as bridges between different graph regions.

During edge matching, SAHEM evaluates potential matches using an edge score that combines the edge weight with a penalty based on separator likelihood. For each candidate edge (u,v), the algorithm computes:

$$\text{score}(u,v) = w(u,v) - \alpha \times \text{penalty}(u,v)$$

The penalty term considers three factors: degree difference between the vertices, neighborhood overlap, and the separator scores of both vertices. The degree difference penalty prevents matching vertices with very different connectivity patterns. The overlap penalty measures how many common neighbors the vertices share relative to their total neighborhoods. The separator penalty directly uses the precomputed separator scores.

This approach aims to avoid matching vertices that are likely to be separators with vertices in the interior of partitions. By preserving separator vertices during coarsening, the algorithm maintains clearer boundaries between different regions of the graph, which can lead to better quality separators when the graph is partitioned at the coarsest level and refined during projection.

Algorithm 7: Separator-Aware Heavy Edge Matching (SAHEM)

input : Graph $G = (V, E)$ with edge weights
output: Matching M and coarser graph

Compute separator likelihood scores:;
foreach *vertex* $v \in V$ **do**
    degree_centrality$[v]$ = degree(v) / $|V|$;
    clustering$[v]$ = clustering coefficient of v;
    sep_score$[v]$ = degree_centrality$[v]$ $\times$ $(1 -$ clustering$[v])$;
end
Initialize matching:;
$M = \emptyset$;
matched = $\{\}$;
Sort vertices by degree (low to high);
Compute separator-aware matching:;
foreach *vertex u in sorted order* **do**
    if $u \notin$ *matched* **then**
        best_score = $-\infty$;
        best_match = null;
        foreach *neighbor v of u* **do**
            if $v \notin$ *matched* ***and*** *weight constraints satisfied* **then**
                edge_score = $w(u, v)$;
                penalty = `ComputePenalty`$(u, v,$sep_score$)$;
                total_score = edge_score $- \alpha \times$ penalty;
                if *total_score* $>$ *best_score* **then**
                    best_score = total_score;
                    best_match = v;
                end
            end
        end
        if *best_match* $\neq$ *null* **then**
            $M = M \cup \{(u,$best_match$)\}$;
            matched = matched $\cup \{u,$best_match$\}$;
        end
    end
end
Create coarser graph by contracting matched edges;
return *Coarser graph*;

Algorithm 8: Edge Cut Score Penalty Computation

input : Vertices u, v, separator scores
output: Penalty score

Degree difference penalty:;
$\text{deg\_diff} = |\text{degree}(u) - \text{degree}(v)| / \max(\text{degree}(u), \text{degree}(v))$;

Neighborhood overlap penalty:;
$\text{common} = |\text{neighbors}(u) \cap \text{neighbors}(v)|$;
$\text{total} = |\text{neighbors}(u) \cup \text{neighbors}(v)|$;
$\text{overlap\_penalty} = 1 - \text{common}/\text{total}$;

Separator penalty:;
$\text{sep\_penalty} = (\text{sep\_score}[u] + \text{sep\_score}[v])/2$;

Combine penalties:;
$\text{penalty} = 0.4 \times \text{deg\_diff} + 0.4 \times \text{overlap\_penalty} + 0.2 \times \text{sep\_penalty}$;
return *penalty*;

3.4. Hypergraph Based Ordering

This section presents a hypergraph-based ordering implementation developed in this thesis. The approach is inspired by the work of [12] and [14], which describe converting a symmetric matrix into Doubly-Bordered Block-Diagonal Form (DB) using hypergraph partitioning. This implementation extends their approach with an efficient method to find edge-clique cover and applies further ordering within the diagonal blocks.

The algorithm begins by constructing a standard graph representation of the symmetric matrix, where vertices correspond to matrix rows/columns and edges represent nonzero entries. From this graph, the algorithm computes an edge-clique cover, which identifies a set of cliques that collectively cover all edges in the graph. Each clique represents a group of vertices that are mutually connected.

The clique-node hypergraph transformation inverts the roles of vertices and cliques. Each clique becomes a node in the hypergraph, and each original graph vertex becomes a hyperedge connecting all cliques that contain it. This transformation enables the use of hypergraph partitioning tools to minimize the number of vertices that span multiple partitions, which naturally produces a vertex separator.

The hypergraph is partitioned using KaHyPar (Karlsruhe Hypergraph Partitioner) into k parts with a small allowed imbalance. The partitioning objective minimizes the connectivity metric, which counts hyperedges that connect nodes from different partitions. Each such hyperedge corresponds to a vertex in the original graph that belongs to multiple cliques assigned to different partitions.

After partitioning the clique-node hypergraph, the algorithm constructs the vertex separator by examining each original graph vertex. A vertex is assigned to partition i if all cliques containing it are assigned to partition i in the hypergraph partition. If a vertex belongs to cliques from multiple partitions, it becomes part of the separator. This

produces k internal regions and one separator region.

To reduce fill-in during factorization, the algorithm applies an ordering method to each diagonal block. The implementation supports AMD, METIS, or nested dissection through the CHOLMOD library. Each diagonal block is extracted as a submatrix, and the chosen ordering algorithm reorders the vertices within that block to minimize fill-in during Cholesky factorization.

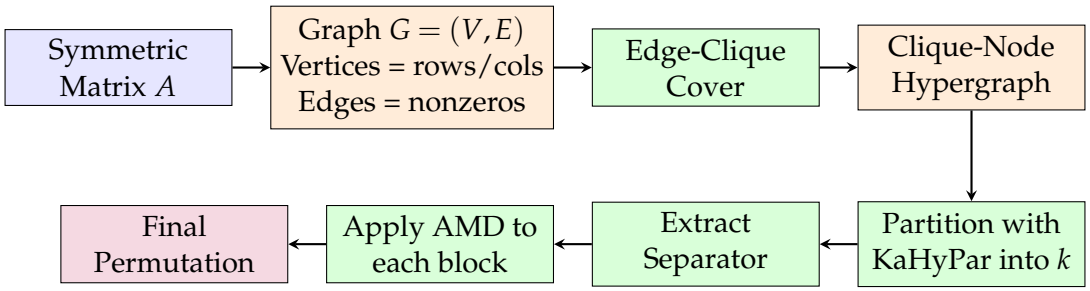

Figure 3.1.: Flowchart of the hypergraph-based symmetric DB form algorithm

The final permutation places all vertices from diagonal block 1, followed by diagonal block 2 through k, with separator vertices at the end. This produces a matrix in symmetric doubly-bordered block-diagonal form, where the diagonal blocks have been optimized for sparse factorization while the off-diagonal structure is confined to the border rows and columns corresponding to the separator.

Algorithm 9: Hypergraph-Based Symmetric DB Form

input : Symmetric matrix A ($n \times n$), number of blocks k
output: Permutation P producing symmetric DB form

Step 1: Create graph representation:;
$G = (V, E)$ where $V = \{1, \ldots, n\}$ and $(i, j) \in E$ if $A_{ij} \neq 0$;

Step 2: Find edge-clique cover:;
Cliques = `FindEdgeCliqueCover`(G);
Build mapping: vertex_to_cliques$[v] = \{c : v \in c, c \in \text{Cliques}\}$;

Step 3: Build clique-node hypergraph:;
`// Each clique becomes a hypergraph node`
`// Each vertex becomes a hyperedge connecting its cliques`
$H = (N, E_H)$ where $|N| = |\text{Cliques}|$;
foreach *vertex* $v \in V$ **do**
    Create hyperedge e_v connecting nodes in vertex_to_cliques$[v]$;
    $E_H = E_H \cup \{e_v\}$;
end

Step 4: Partition hypergraph:;
clique_partition = `PartitionHypergraph`(H, k) using KaHyPar;

Step 5: Extract vertex separator:;
Initialize Parts$[1..k] = \emptyset$, Separator $= \emptyset$;
foreach *vertex* $v \in V$ **do**
    partitions $= \{\text{clique\_partition}[c] : c \in \text{vertex\_to\_cliques}[v]\}$;
    if $|partitions| = 1$ **then**
        $p =$ the single partition in partitions;
        Parts$[p] =$ Parts$[p] \cup \{v\}$;
    end
    else
        Separator $=$ Separator $\cup \{v\}$;
    end
end

Step 6: Apply AMD to each diagonal block:;
foreach *part* $i = 1$ *to* k **do**
    $A_i = A[\text{Parts}[i], \text{Parts}[i]]$ `// Extract diagonal block`
    perm$_i =$ `ApplyAMD`(A_i) `// Order using AMD/METIS/etc.`
    Reorder Parts$[i]$ according to perm$_i$;
end

Step 7: Build final permutation:;
$P = [\text{Parts}[1], \text{Parts}[2], \ldots, \text{Parts}[k], \text{Separator}]$;
return P;

Algorithm 10: Edge-Clique Cover (Greedy Heuristic)

input : Graph $G = (V, E)$
output: Set of cliques covering all edges

```
Cliques = ∅;
covered_edges = ∅;
Find maximal cliques:;
maximal_cliques = all maximal cliques in G;
Add cliques that cover new edges:;
foreach clique C in maximal_cliques do
    clique_edges = {(u,v) : u,v ∈ C, u < v, (u,v) ∈ E};
    new_edges = clique_edges \ covered_edges;
    if new_edges ≠ ∅ then
        Cliques = Cliques ∪ {C};
        covered_edges = covered_edges ∪ clique_edges;
    end
end
Cover remaining edges with 2-cliques:;
remaining = E \ covered_edges;
foreach edge (u,v) ∈ remaining do
    Cliques = Cliques ∪ {{u,v}};
end
return Cliques;
```

3.5. GPU Implementation of RCM

Reverse Cuthill-McKee (RCM) can be thought of slightly differently and implemented given an efficient breadth-first search (BFS) function. The RCM algorithm is simply BFS with two modifications: (1) neighbors are visited in degree-sorted order, and (2) the final ordering is reversed. This structure allows us to wrap an existing GPU BFS implementation with preprocessing and postprocessing steps.

Algorithm 11: GPU RCM Implementation

input : Graph $G = (V, E)$ in CSR format
output: RCM permutation P

Preprocessing: Sort adjacency lists;
foreach *vertex* $u \in V$ ***in parallel on GPU*** **do**
    `SortNeighborsByDegree`(u) `// Parallely sort neighbors`
end
Core traversal: Run BFS with sorted neighbors;
order $= [\,]$;
visited $= \{\}$;
foreach *component start vertex s (by increasing degree)* **do**
    if $s \notin$ *visited* **then**
        comp_order $=$ `GPU_BFS`(G, s) `// BFS from source` s
        visited $=$ visited $\cup$ comp_order;
        order $=$ order $+$ comp_order;
    end
end
Postprocessing: Reverse the ordering;
$P =$ `Reverse`(order);
return P;

The GPU BFS was originally developed by NVIDIA in [15]. We work with one of the latest implementations of GPU BFS in [16]. The GPU BFS uses a level-synchronous approach that processes the graph one level at a time. Starting from a source vertex, the algorithm maintains a frontier of vertices to explore at the current level. Each iteration consists of two phases: expansion and contraction. In the expansion phase, all neighbors of frontier vertices are gathered in parallel by reading adjacency lists from CSR format. Since the adjacency lists were presorted by degree, neighbors are naturally visited in the correct RCM order. Multiple threads cooperatively read adjacency lists, with different parallelization strategies used based on vertex degree—single threads for low-degree vertices, entire warps (32 threads) for medium-degree vertices, and full thread blocks for high-degree vertices. In the contraction phase, the algorithm filters the gathered neighbors to remove duplicates and already-visited vertices using atomic compare-and-swap operations, producing the next level's frontier. This process repeats until the frontier becomes empty, at which point the BFS traversal is complete.

This GPU RCM implementation adapts the parallel BFS from the NVIDIA CUDA SDK [16]. The modifications are just by having a preprocessing step before BFS and reversing the result after BFS.

Chapter 4

Results

In this chapter, we first describe our evaluation setup, which consists of the HPC cluster used for our experiments, the matrix datasets, and the algorithmic implementations evaluated. We then present a detailed analysis of various performance metrics, including execution time, memory usage, parallelization and matrix fill-in reduction.

4.1. Evaluation setup

Everything that is evaluated is ran on Fritz, a high-performance computing cluster at NHR@FAU.

4.1.1. Hardware Infrastructure

Fritz is a parallel CPU cluster operated by NHR@FAU, featuring Intel Ice Lake and Sapphire Rapids processors with an InfiniBand (IB) network and a Lustre-based parallel filesystem accessible under `$FASTTMP`. The cluster configuration consists of:

Nodes	**CPUs and Cores**	**Memory**	**Slurm Partition**
992	2 × Intel Xeon Platinum 8360Y (Ice Lake) 2 × 36 cores @2.4 GHz	256 GB	singlenode, multinode
48	2 × Intel Xeon Platinum 8470 (Sapphire Rapids) 2 × 52 cores @2.0 GHz	1 TB	spr1tb
16	2 × Intel Xeon Platinum 8470 (Sapphire Rapids) 2 × 52 cores @2.0 GHz	2 TB	spr2tb

Table 4.1.: Fritz cluster node configuration

The login nodes fritz[1-4] are equipped with 2 × Intel Xeon Platinum 8360Y (Ice Lake) processors and 512 GB main memory. Additionally, the remote visualization node fviz1 features 2 × Intel Xeon Platinum 8360Y processors with 1 TB main memory, one Nvidia A16 GPU, and 30 TB of local NVMe SSD storage.

4.2. Matrices dataset

We selected a diverse set of sparse matrices from the SuiteSparse Matrix Collection and our custom dataset of matrices encountered in Quantum Transport to evaluate our implementations. The SuiteSparse matrices are chosen to cover a variety of application domains, including computational fluid dynamics (CFD), chemistry, circuit simulation, graph analysis, optimization, and structural engineering. We have listed the matrices alongside their respective groups, number of vertices, and number of edges in Table 4.2. The Quantum Transport matrices are listed in Table 4.3.

Graph name	Group	No. of vertices	No. of edges
copter2	CFD	55476	407714
ex10	CFD	2410	28625
parabolic_fem	CFD	525825	2100225
3Dspectralwave	Chemistry	680943	17165766
CO	Chemistry	221119	3943588
crystk03	Chemistry	24696	887937
Ga19As19H42	Chemistry	133123	4508981
Si87H76	Chemistry	240369	5451000
SiH4	Chemistry	5041	88472
circuit_3	Circuit	12127	48137
G2_circuit	Circuit	150102	438388
memplus	Circuit	17758	126150
rajat06	Circuit	10922	28922
rajat10	Circuit	30202	80202
rajat15	Circuit	37261	443573
144	Graphs	144649	1074393
598a	Graphs	110971	741934
auto	Graphs	448695	3314611
ca-AstroPh	Graphs	18772	198110
citationCiteseer	Graphs	268495	1156647
delaunay_n20	Graphs	1048576	3145686
dictionary28	Graphs	52652	89038
boyd2	Optimizations	466316	890091
c-55	Optimizations	32780	218115
c-70	Optimizations	68924	363955
gupta2	Optimizations	62064	2155175

Continued on next page

Graph name	Group	No. of vertices	No. of edges
gupta3	Optimizations	16783	4670105
lpl1	Optimizations	32460	180248
ncvxbqp1	Optimizations	50000	199984
apache1	Structural	80800	311492
apache2	Structural	715176	2766523
nasasrb	Structural	54870	1366097

Table 4.2.: SuiteSparse matrix dataset used for evaluation

Table 4.3.: Quantum Transport matrix dataset used for evaluation

Graph name	No. of vertices	No. of edges	Description
airpoll_conditional_st3	8499	1218651	Spatio-temporal statistical Modelling
airpoll_prior_st3	8499	1205931	Spatio-temporal statistical Modelling
cnt_cp2k	9152	6154350	DFT Hamiltonian of Carbon Nanotube
cnt_w90	768	71680	DFT Hamiltonian of Carbon Nanotube
kmc_potential_0	403605	10007089	Kinetic Monte Carlo for Device Modelling
kmc_potential_1	1632355	41208963	Kinetic Monte Carlo for Device Modelling
qubit_fem_b4	116380	2517228	FEM Matrix for Qubit
sinw_w90	7488	5310160	DFT Hamiltonian of Silicon Nanowire

4.3. Methodology

For our evaluation, we systematically assessed the performance of eleven different reordering algorithms across all matrices listed in Tables 4.2 and 4.3. The evaluated algorithms encompass both sequential and parallel approaches, ranging from classical degree-based methods to graph partitioning and hypergraph-based techniques:

1. **Classical Methods:**
   - AMD (Approximate Minimum Degree)
   - COLAMD (Column Approximate Minimum Degree)
   - RCM (Reverse Cuthill-McKee)
   - Natural (Original matrix ordering - baseline)
2. **Graph Partitioning Methods:**
   - METIS (Sequential graph partitioning-based reordering)
   - METIS+IC (METIS with custom coarsening integration)
   - SCOTCH (Sequential graph partitioning)
   - PT-SCOTCH (Parallel graph partitioning)
   - ParMETIS (Parallel graph partitioning)
3. **Hypergraph-based Methods:**

- HG-2 , HG-4 , HG-8 , HG-16 (Hypergraph-based reordering with block partition sizes of 2, 4, 8, and 16 vertices respectively)

The hypergraph-based methods (HG-2, HG-4, HG-8, HG-16) employ different block partition sizes to explore the trade-off between computational complexity and reordering/parallelization quality. All these algorithms are described in detail in Chapter 3. The highlighted methods indicate our own implementations.

4.3.1. Performance Metrics

Our comprehensive evaluation measures five key performance indicators to assess the effectiveness of each reordering algorithm:

Fill-in Reduction: We measure the number of non-zero entries introduced during symbolic Cholesky factorization using the `cmpfillin` binary provided by the METIS library. This tool performs symbolic factorization (as described in Chapter 2) to count the additional non-zero entries without executing the actual numerical computation.

Reordering Time: The wall-clock time required to compute the reordering itself is measured using Python's `time.perf_counter()` with microsecond precision. This overhead cost is crucial for understanding the practical applicability of each method.

Memory Usage: We implement a dedicated memory monitoring system using a separate thread that samples memory consumption every 50 milliseconds during reordering operations. The monitoring captures both peak memory usage (maximum RSS observed) and average memory consumption throughout the reordering process. Memory measurements are obtained via the `psutil` library, tracking the resident set size (RSS) of the process and computing the memory increase relative to a baseline measured before algorithm execution.

Parallelization Potential: We assess the elimination tree depth as an indicator of the inherent parallelism available in the factorization. As mentioned in Chapter 2, the elimination tree is constructed by identifying parent-child relationships in the symbolic factorization structure, where the tree depth represents the critical path length and thus the theoretical lower bound on parallel factorization time.

For memory profiling, we initially attempted to use the Massif profiler from Valgrind, but encountered issues with our Python-based implementations and the cluster environment. Consequently, we developed a custom memory measurement protocol that employs a thread-safe monitoring system to capture accurate memory usage patterns during reordering operations.

Our memory measurement implementation works by first establishing a baseline memory consumption before starting any reordering algorithm, recording the initial resident set size (RSS) using `psutil.Process().memory_info().rss`. During algorithm

execution, a dedicated monitoring thread runs concurrently, sampling memory usage every 50 milliseconds throughout the entire operation. This thread continuously updates the maximum observed memory consumption and maintains a comprehensive list of all samples for subsequent average computation.

Upon completion of the reordering algorithm, we compute both the peak memory increase (calculated as the maximum observed RSS minus the baseline) and the average memory increase (computed as the mean of all samples minus the baseline), with results reported in kilobytes. For cases where the monitoring thread fails to capture meaningful data, such as very fast operations that complete before sufficient samples can be collected, we provide conservative estimates based on matrix characteristics, using approximately 100% of the matrix storage size as an upper bound for memory consumption.

All experiments are executed on the Fritz cluster to ensure consistent hardware conditions across all measurements. Each algorithm is tested on every matrix in our dataset, and results are averaged over five independent runs to mitigate variability.

4.4. Evaluation

For each matrix in our dataset with different reordering algorithms applied, we have collected all the aforementioned metrics, and these can be found in our appendix/supplementary material A. Here, we present results and visualizations for our underlying metrics for some of them.

Figure 4.1 presents a comparative analysis of fill-in reduction across different matrix categories, showing the ratio of fill-in to original non-zeros for representative matrices from each domain. This visualization demonstrates how reordering effectiveness varies significantly across different problem types and matrix structures.

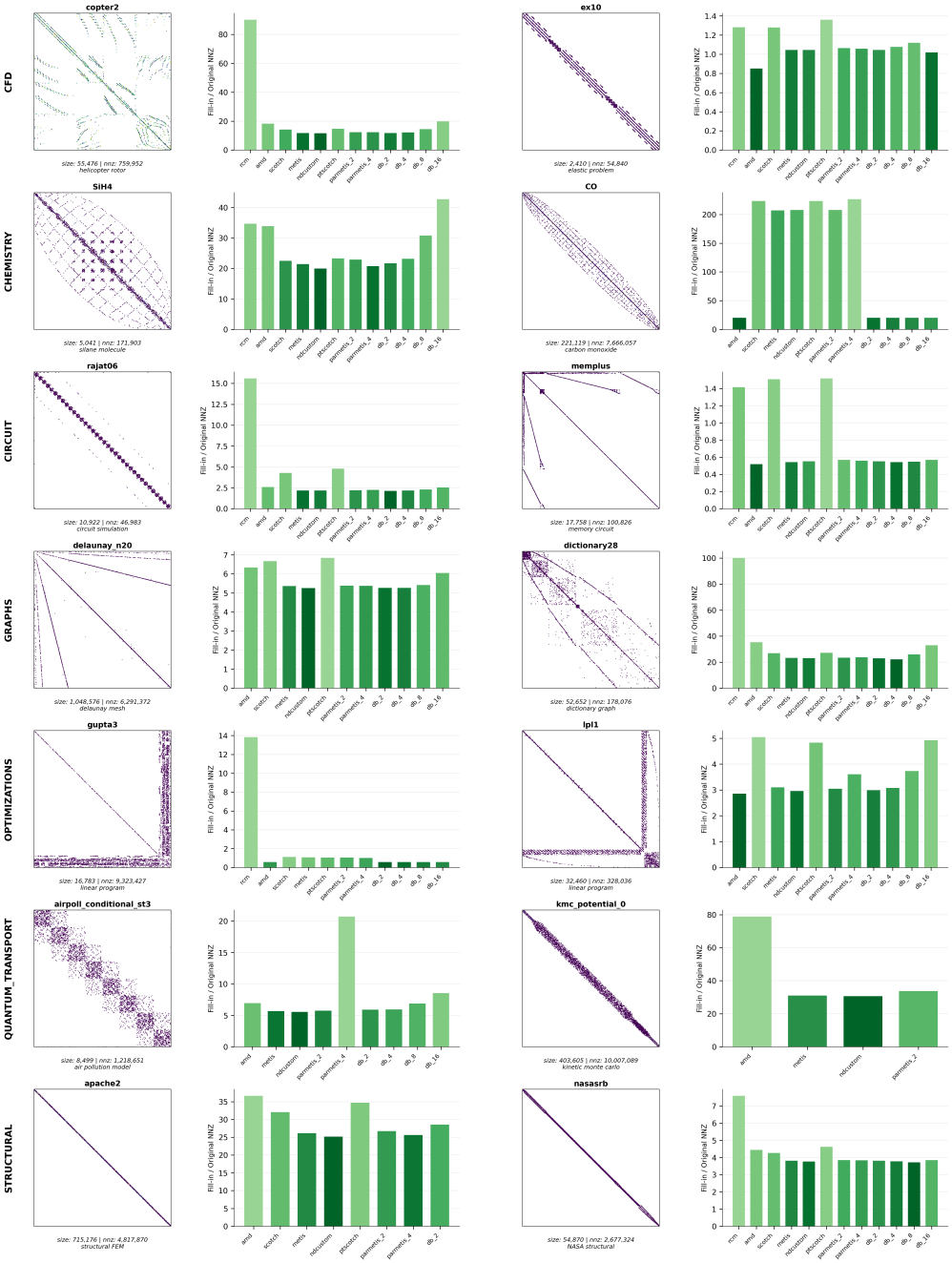

Figure 4.1.: Fill-in ratio (fill-in/original nnz) comparison across different matrix categories

Our experimental results reveal distinct performance patterns across different matrix domains and algorithm categories. The hypergraph-based methods, METIS, and our custom METIS implementation with improved coarsening (METIS+IC) show strong

performance with lower fill-in reduction compared to classical methods. These methods achieve 30-60% lower fill-in values than traditional approaches like AMD and COLAMD across most domains. Among the hypergraph methods, smaller partition sizes (HG-2 and HG-4) typically produce optimal results, while larger partitions are ineffective. Our custom METIS+IC implementation demonstrates that enhanced coarsening strategies can achieve performance comparable to hypergraph methods. SCOTCH and PT-SCOTCH show moderate improvements over classical methods but do not match the quality of METIS-based approaches.

Domain-specific analysis reveals that hypergraph methods, METIS, and METIS+IC perform well in circuit and graph problems, where they achieve 35-50% fill-in reduction compared to AMD. For CFD matrices, these advanced methods show modest but consistent improvements (10-30%), while chemistry matrices present scalability challenges where many classical methods fail on the largest instances, leaving primarily METIS-based or classical methods viable. The optimization and structural domains show variable performance depending on problem structure, with hypergraph methods and METIS variants providing 10-25% improvements in most cases.

Figure 4.2 presents the scaling behavior of reordering algorithms with respect to the number of non-zero entries. This graph shows the time required for each algorithm to complete and how it scales with increasing non-zero counts.

The reordering time results show notable performance differences across methods. RCM and AMD are the fastest options, with RCM typically completing in under one second (0.006-0.76s) across all matrix sizes and AMD performing well for small-to-medium matrices (0.046-2.09s). SCOTCH and METIS generally complete within reasonable timeframes (under 50 seconds), while parallel methods like ParMETIS and PT-SCOTCH have higher overhead that may be justified for larger problems. The hypergraph partitioning methods (HG variants) require considerably more time, with some executions taking over 270 seconds.

Regarding scalability with increasing NNZ, the methods exhibit different growth patterns. AMD shows sublinear scaling (slope 0.52), which becomes more favorable as matrix size increases, while RCM maintains near-linear scaling (slope 0.72) with consistent performance characteristics. SCOTCH demonstrates reasonable scaling (slope 0.65), and the ParMETIS variants maintain moderate complexity (slopes 0.64-0.68) despite their higher base execution times. METIS+IC shows superlinear scaling (slope 1.14) due to its modified coarsening approach, which becomes problematic for very large matrices, while METIS approaches linear scaling (slope 0.81). The HG hypergraph methods show scaling slopes between 0.71-0.76, though their high absolute execution times remain a concern.

The results indicate that simpler methods like AMD and RCM provide favorable execution times compared to more complex approaches for large-scale sparse matrix reordering. While parallel methods may become advantageous for extremely large problems, the hypergraph partitioning approaches have higher computational costs relative to their fill-in benefits in typical sparse matrix applications.

We then now look at the elimination tree depth as a measure of parallelism. Similar to fill-in, we sample randomly two matrices from different domains to show the elimination

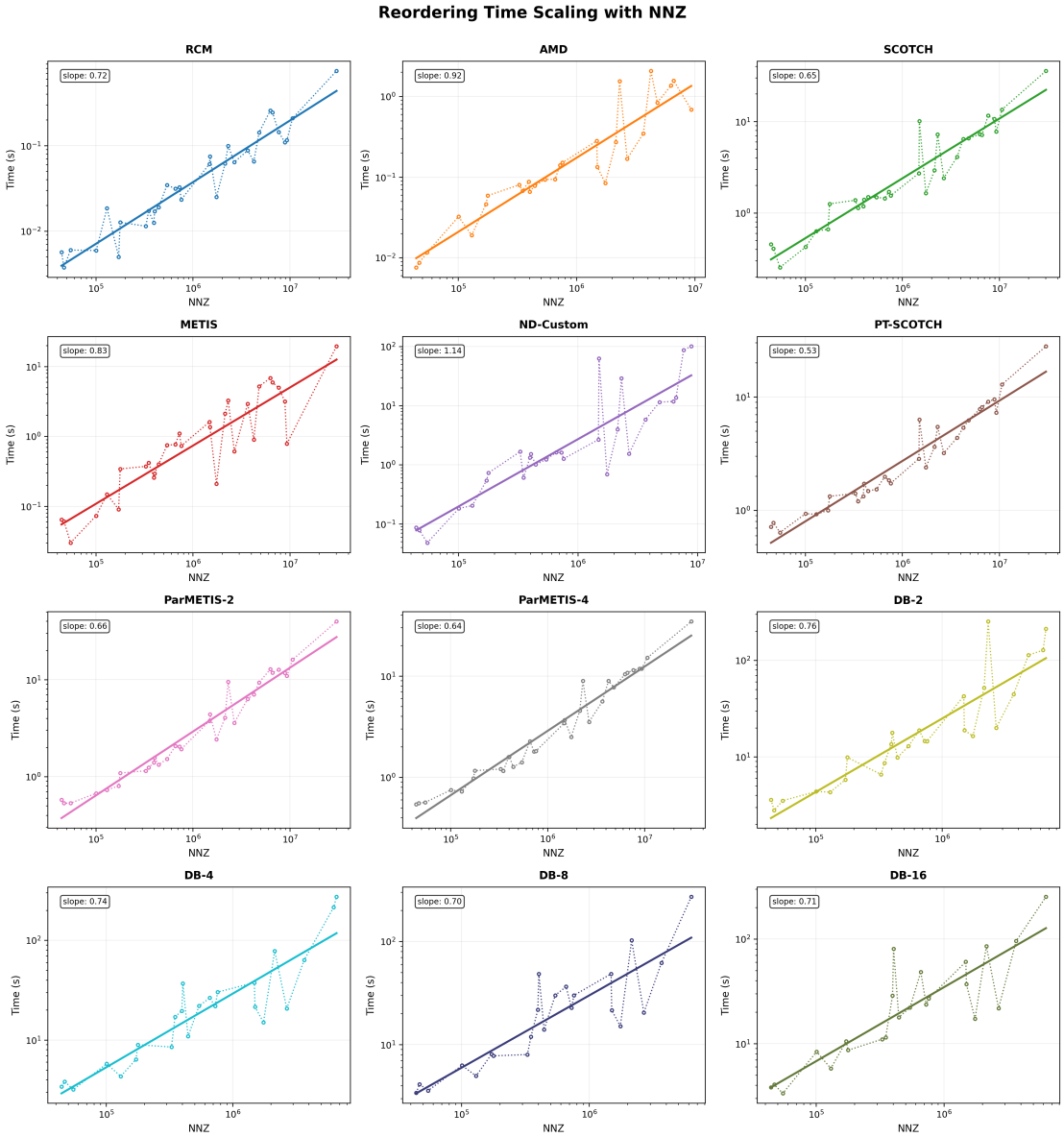

Figure 4.2.: Reordering time scaling with matrix size (number of non-zeros) for different algorithms. Each subplot shows the relationship between matrix size and computational time for various reordering methods.

tree depth for different reordering algorithms.

The elimination tree depth results provide insight into the parallelization potential of different reordering methods, as shallower trees enable more parallel execution during factorization. The parallel methods show advantages in reducing tree depth compared to sequential approaches. ParMETIS variants produce shallow elimination trees, with

ParMETIS-2 and ParMETIS-4 achieving depths in the range of 14-42 across various matrices, while ParMETIS-8 and ParMETIS-16 maintain depths between 25-50. METIS also performs well for parallelization potential, producing trees with depths around 22-160, which represents a significant improvement over many sequential methods.

Sequential methods show mixed results for parallelization potential. AMD typically produces tree depths ranging from very shallow (4-20) for some matrices to quite deep (250-830) for others, making its parallelization benefits matrix-dependent. NDCUSTOM, being METIS with modified coarsening, generally produces similar tree depths to METIS, typically ranging from 24-171, though it can produce deeper trees (up to 839) for some matrices, suggesting that the coarsening modification does not improve parallelization potential across all cases. RCM produces the deepest trees among the methods tested, with depths exceeding 300-400 and reaching over 700 for some matrices, which limits parallel factorization opportunities. SCOTCH performs moderately, with tree depths generally ranging from 23-290, while PT-SCOTCH shows improved parallelization potential with depths typically between 54-328, though it can produce very deep trees exceeding 700.

The hypergraph partitioning methods (DB variants) show variable performance for parallelization, with tree depths ranging from 19-301 depending on the number of partitions used. DB-2 often produces deeper trees (49-603), while DB-16 tends toward moderate depths (66-830), though the relationship between partition count and tree depth is not always consistent. Natural ordering predictably produces very deep trees (often 200-800+), confirming the necessity of reordering for parallel factorization. The results indicate that while parallel reordering methods require more computational time, they provide substantial benefits for subsequent parallel factorization phases through significantly reduced elimination tree depths.

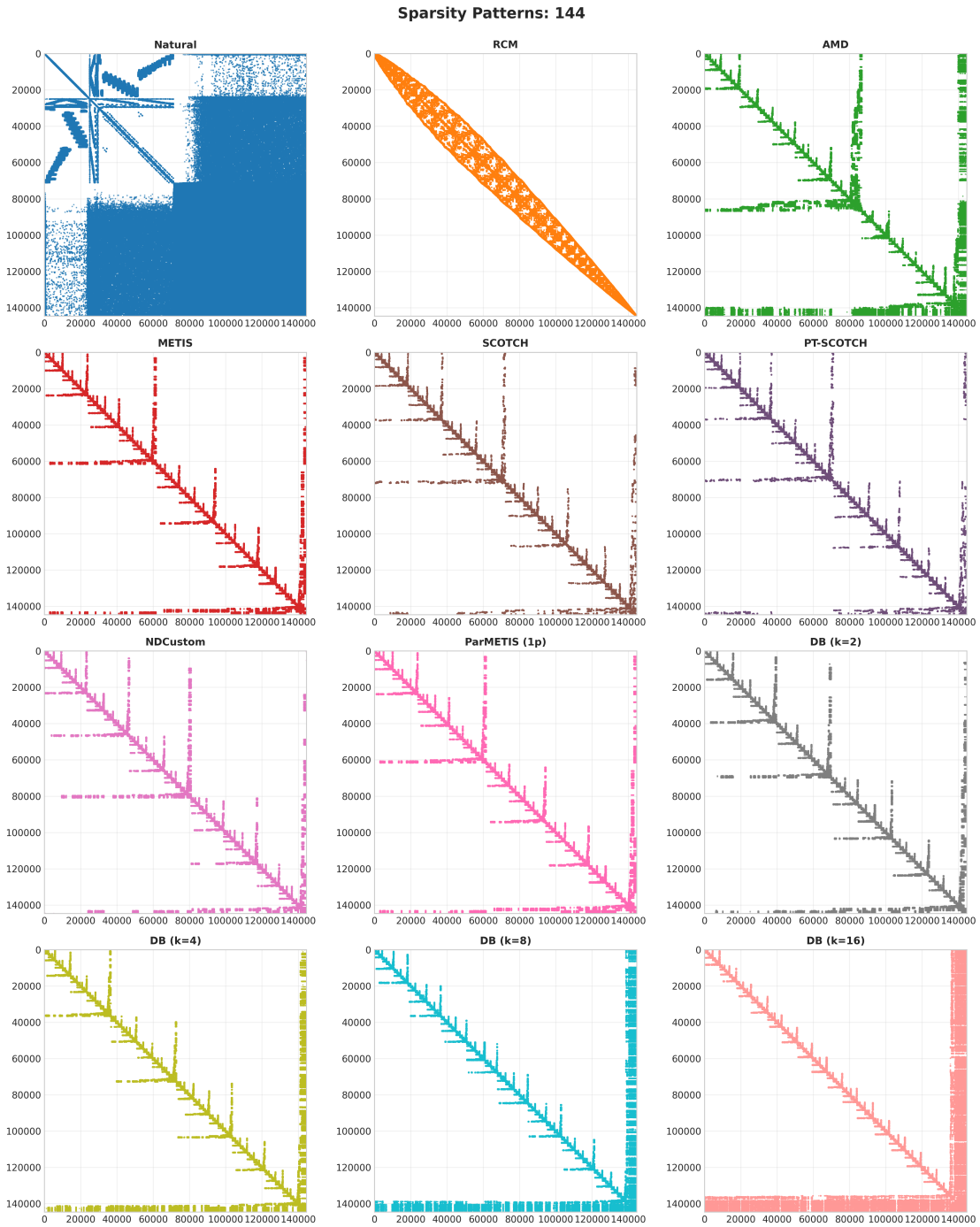

Figure 4.3.: Sparsity patterns of matrix 144 with different reordering algorithms applied. The natural ordering (top-left) shows a scattered pattern leading to high fill-in, while optimized reorderings (other panels) demonstrate more defined structures.

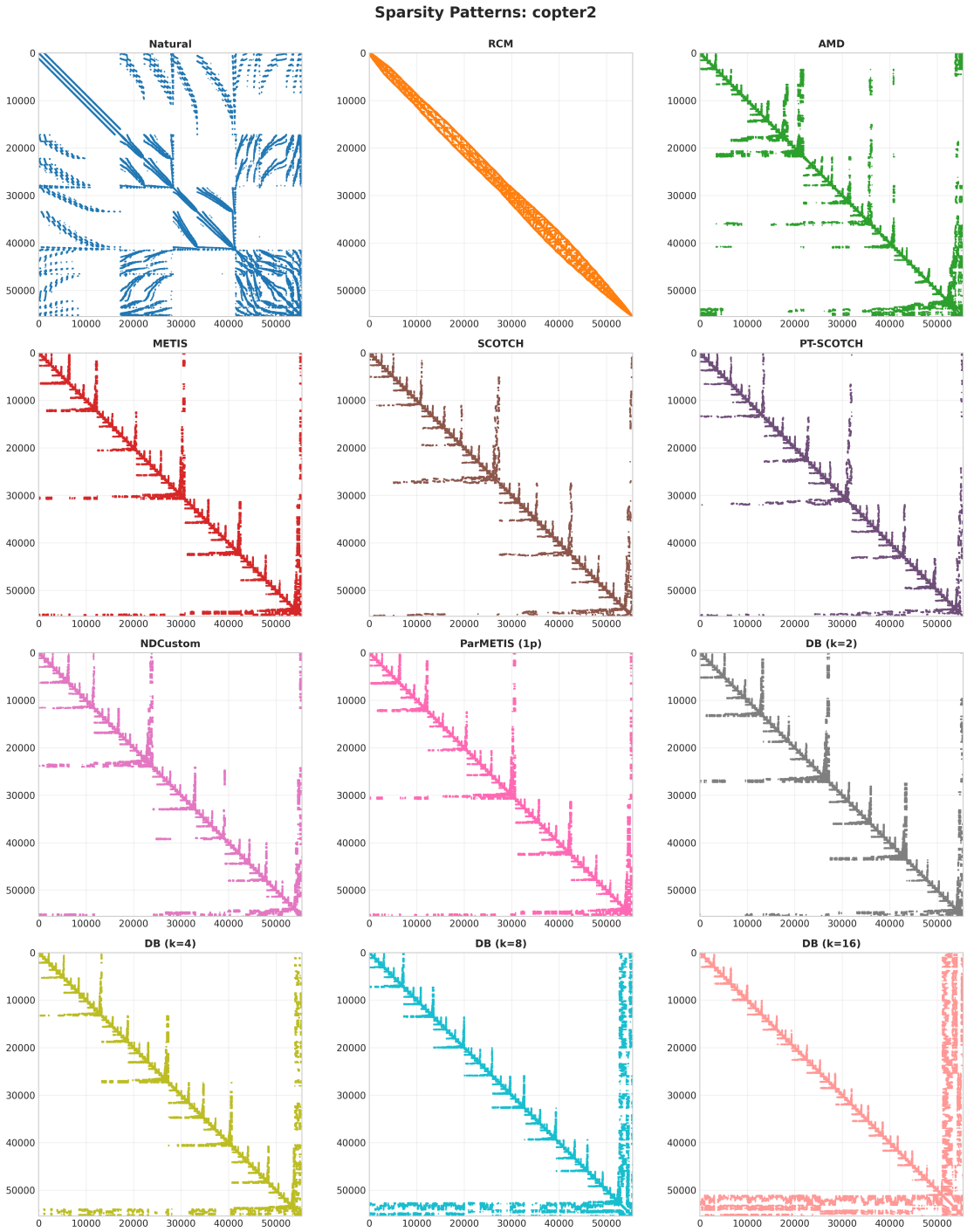

Figure 4.4.: Similarly, sparsity patterns of matrix copter2 with different reordering algorithms applied.

Figure 4.5.: Elimination tree depth comparison across different matrix categories for various reordering algorithms. Lower depth indicates better parallelization potential. Blue indicates lower depth (better), while pink indicates higher depth (worse).

4.4.1. GPU-accelerated RCM

In this section, we present the performance of our GPU-accelerated implementation of the Reverse Cuthill-McKee (RCM) algorithm compared to a traditional CPU-based implementation. We measure only the runtime of the RCM algorithm and not the fill-in, as the quality of the ordering produced by both implementations is identical. We test these implementations of a different hardware setup, as the Fritz cluster does not have suitable GPU nodes. Instead, we used the "alex" cluster, which provides GPU acceleration capabilities. The alex cluster consists of 44 nodes equipped with 2 × AMD EPYC 7713 "Milan" processors running at 2.0 GHz, featuring 8 × NVIDIA A100 GPUs (with 40 GB or 80 GB HBM2 memory), 1024 GB or 2048 GB system memory, 14TB local NVMe SSD storage, and HDR200 Infiniband networking. Additionally, 38 nodes contain the same processors with 8 × NVIDIA A40 GPUs (48 GB DDR6 memory), 512 GB system memory, and 7 TB local NVMe SSD storage.

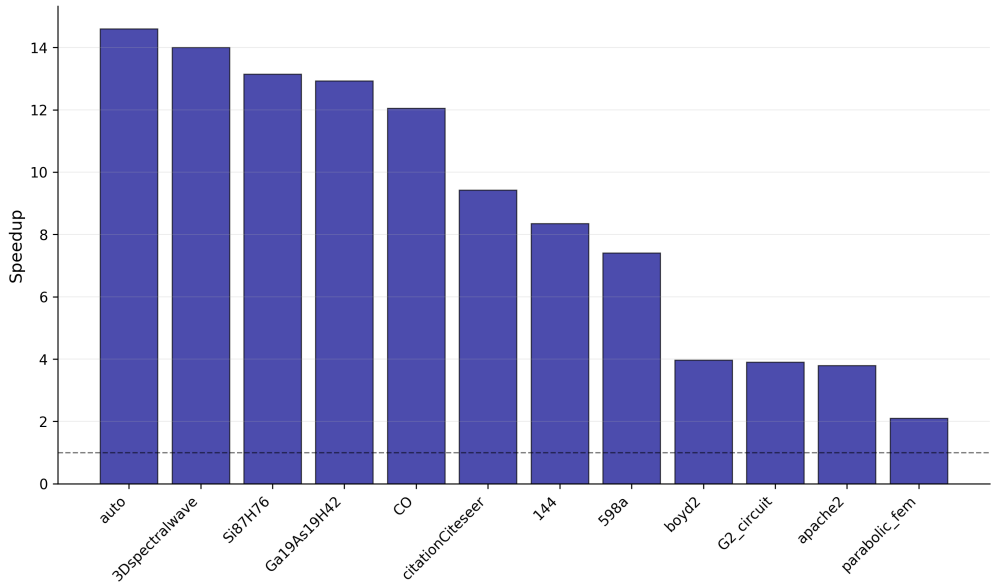

Figure 4.6.: Speedup of GPU-accelerated RCM compared to CPU-based RCM on large matrices (over 100K nodes).

For small matrices, the overhead of data transfer to and from the GPU negates any performance benefits, resulting in slower execution times compared to the CPU implementation. However, as matrix sizes increase, the GPU-accelerated RCM demonstrates significant performance improvements. In our experiments, we observe speedups ranging from 1.6x to 14.6x for matrices larger than 100,000 nodes. Some irregular matrices, such as `c-70` and `gupta3`, exhibit particularly high speedups of 19.7x and 15.6x respectively, even though they are smaller than 100,000 nodes. Profiling indicated that the majority time of the GPU implementation for these matrices was spent in the preprocessing phases, suggesting that structures of the matrices can influence performance.

4.5. Current limitations

Our evaluation has important limitations that should be acknowledged. First, our analysis is not exhaustive—we evaluated only a subset of available sparse matrix reordering algorithms and libraries, focusing on the most commonly used and representative methods. Additionally, our memory measurement system faced significant challenges: the monitoring thread frequently failed to capture meaningful data for fast-completing algorithms or when external binaries changed process IDs (particularly with hypergraph methods). For several large matrices, symbolic factorization failed due to memory constraints, preventing complete evaluation of all methods across our entire dataset.

The practical applicability of some methods is also limited by performance constraints. Hypergraph-based methods, while sometimes producing high-quality reorderings, proved computationally expensive and impractical for large matrices. Furthermore, our GPU acceleration efforts were limited to the RCM algorithm—we did not implement GPU versions of other reordering methods, which represents a significant opportunity for future performance improvements across the entire algorithm suite.

Chapter 5

Other Approaches

In this chapter, we explore alternative and promising approaches to the sparse matrix reordering problem beyond traditional heuristic methods. These methods were found by myself to be either computationally difficult to scale for large matrices or were found to have some bottlenecks, but nevertheless represent interesting directions for future work.

5.1. Graph Reinforcement Learning for Reordering

As we know that sparse symmetric matrices can be represented as undirected graphs, it seems promising that this representation allows GNNs to naturally capture the local neighborhood relationships that classical ordering heuristics rely on, such as node degree and clustering patterns.

Traditional heuristics like minimum degree ordering make greedy decisions based on limited local information. There has been a few approaches for using machine learning to learn better heuristics, such as the work by [13], which uses CNN and they tackle large matrices by partitioning the graph.

GNNs, however, can propagate information across multiple hops in the graph, enabling each node to consider not just its immediate neighbors but also the broader structural context. It also allows us to have variable sized graphs. This multi-hop reasoning capability allows the network to anticipate how eliminating one node will affect distant parts of the matrix, potentially leading to more effective ordering decisions.

The message-passing architecture of GNNs naturally models the fill-in process during matrix factorization. When a node is eliminated, it creates new connections between its neighbors, which GNNs can represent through their aggregation and update mechanisms. The network can learn to predict these fill-in patterns and make elimination choices that minimize overall structural complexity.

The graph neural network, as shown in Figure 5.1, processes the sparse matrix represented as a graph, computing embeddings for each node based on features such as degree, clustering coefficient, and centrality measures. The actor network uses these

embeddings to select which node to eliminate next, while the critic network estimates the value of the current state. The agent receives rewards based on the fill-in generated at each step, with penalties for creating new edges and bonuses for efficient elimination patterns.

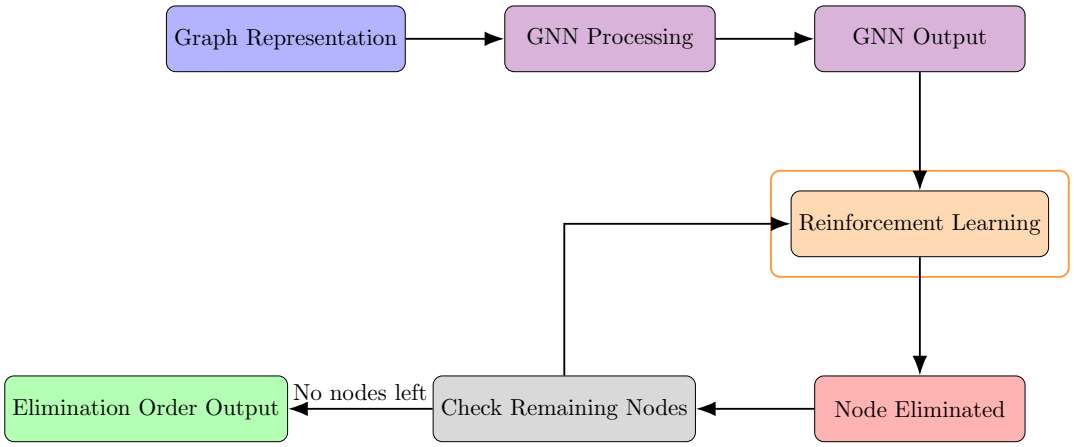

Figure 5.1.: Reinforcement Learning Framework for Sparse Matrix Reordering using GNNs

The model shows good and promising results on small matrices, achieving 9.8% improvement over RCM and 81.4% improvement over MinDegree on the ash85 matrix, and 28.4% and 51.0% improvements respectively on the bcsstk22 matrix. Furthermore, experiments on synthetic graphs with a few hundred nodes demonstrated good results, suggesting the approach can handle moderately sized problems. However, the method struggles to scale to very large matrices due to the computational complexity of training GNNs on large graphs. Future work can explore scaling techniques such as graph coarsening, hierarchical approaches, or coarser representations of the graph to make it feasible for larger matrices.

5.2. GPU Accelerated Nested Dissection

There is very limited work on GPU-accelerated reordering algorithms. I had presented earlier in this thesis, a GPU implementation of the RCM algorithm. Another promising approach is to implement the nested dissection algorithm on GPUs. One such approach is presented by [17], which leverages a GPU-based geometry processing library to perform fast graph partitioning, a key step in nested dissetion. The method achieves sigificant speedups over the tradition4al CPU-based METIS library but the quality of the ordering is around 3 to 8 times worse than METIS, in their experiments.

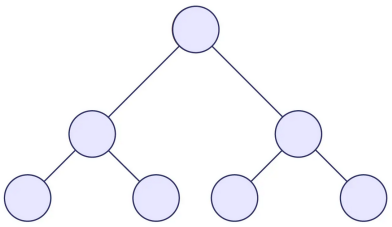

Figure 5.2.: Recursive calls

The primary bottleneck in running nested dissection on GPUs is the recursive nature of the algorithm. Each level of recursion requires partitioning the graph and identifying separators. We leveraged a graph processing library, Jet, which is a multilevel graph partitioning library designed for GPU [18]. The library comes with an efficient implementation of k-way partitioning done using a parallel multilevel approach. One can do a 2-way partitioning by setting k=2, but unsurprisingly, it performs worse in run-time as each call/partition (circle in Figure 5.2) is done sequentially. Another approach was to use k = 2^d, where d is the depth of recursion such each subgraph reaches the threshold size after d levels of recursion. This approach is similar to the approach done using Hypergraph partitioning as mentioned in Chapter 3, in the way that the partition divides the graph into smaller subgraphs and the cumulative separators found are placed at the end, producing sparsity-pattern similar to hypergraph based methods in Chapter 3. This method, which is questionable to call it Nested Dissection, however produces orderings faster than METIS for large graphs but the quality of the ordering is still not comparable to METIS expectedly as you get better separators when you do recursive bisection than a single k-way partitioning. Such an approach produces orderings that are around 2 to 3 times worse than METIS in my experiments on large matrices (`parabolic_fem.graph` and `auto.graph`) but the speedups are significant around 5 to 6 times tested on the same environment as mentioned in Chapter 4.

Chapter 6

Conclusion and Future Work

This thesis presented a comprehensive evaluation of sparse symmetric matrix reordering algorithms across diverse matrix structures and application domains. Through systematic benchmarking on the Fritz HPC cluster, we assessed many reordering algorithms, ranging from classical degree-based methods to newer graph partitioning and hypergraph-based techniques, across multiple performance metrics including fill-in reduction, computational efficiency, memory consumption, and parallelization potential.

Our evaluation reveals that advanced methods such as METIS, SCOTCH, and hypergraph based approaches consistently outperform classical algorithms like AMD and RCM in terms of fill-in reduction, achieving 30-60% fewer fill-ins across most domains. Among the hypergraph methods, smaller partition sizes (HG-2 and HG-4) demonstrate superior effectiveness. Our custom METIS implementation with improved coarsening (METIS+IC) validates the benefits of enhanced coarsening strategies, producing results competitive with the best hypergraph methods. However, this improvement comes at a computational cost. Hypergraph methods require significantly more time (up to 270 seconds), while simpler methods like RCM complete in under one second.

In the course of this work, we implemented several efficient variants of existing algorithms. Our GPU-accelerated RCM implementation demonstrates substantial speedups over CPU-based versions for large matrices. The METIS+IC variant, incorporating refined coarsening strategies, achieves fill-in quality comparable to more complex hypergraph methods while maintaining reasonable execution times. We also explored hypergraph-based reordering methods that exploit block structures in matrices, showing promise particularly for circuit and graph problems.

Several promising directions remain for future investigation. Machine learning approaches, particularly graph neural networks (GNNs), show encouraging results on small matrices but require techniques like coarsening or hierarchical representations to scale to larger problems. Reordering algorithms for emerging architectures also warrant further research, while we implemented GPU-accelerated RCM, extending GPU implementations to nested dissection, minimum degree variants, and hypergraph methods could yield significant performance improvements. Finally, our evaluation re-

veals that algorithm effectiveness varies significantly across matrix domains, suggesting that adaptive schemes which automatically select or tune algorithms based on matrix characteristics could improve performance across diverse applications.

Appendix A

Experimental Results

This appendix presents the complete experimental results for all matrix reordering algorithms evaluated in this thesis.

Table A.1 presents the number of nonzero entries after factorization for each reordering method. Table A.2 presents the computational time in seconds required to compute each reordering. Lower values indicate faster reordering algorithms. Table A.3 presents the peak memory usage in kilobytes during the reordering computation. Lower values indicate better memory efficiency. Table A.4 presents the average memory usage in kilobytes during the reordering computation. Table A.5 presents the depth of the elimination tree produced by each reordering. Lower depths generally indicate better potential for parallel factorization.

Empty or zero cells indicate that the algorithm either failed to complete, exceeded memory limits, timed out or some computation error. All measurements were performed on identical hardware configurations to ensure fair comparison. There are some meaningless values for memory usage, especially for hypergraph methods, for example showing as 4KB, very likely caused by failing the capture the memory usage for the corresponding PID process.

Matrix	Natural	RCM	AMD	METIS	NDCustom	ParMETIS-2	ParMETIS-4	ParMETIS-8	SCOTCH	PT-SCOTCH	db-2	db-4	db-8	db-16
144	1.8×10^{19}	9.3×10^{8}	9.3×10^{7}	4.7×10^{7}	4.6×10^{7}	4.7×10^{7}	4.8×10^{7}	4.8×10^{7}	5.1×10^{7}	5.3×10^{7}	4.7×10^{7}	4.7×10^{7}	5.2×10^{7}	6.8×10^{7}
3Dspectralwave	1.8×10^{19}	—	—	1.3×10^{9}	—	1.3×10^{9}	1.4×10^{9}	1.5×10^{9}	1.4×10^{9}	2.0×10^{9}	1.8×10^{19}	1.8×10^{19}	1.8×10^{19}	1.8×10^{19}
598a	—	—	4.6×10^{7}	2.5×10^{7}	2.5×10^{7}	2.5×10^{7}	2.6×10^{7}	2.6×10^{7}	2.9×10^{7}	2.9×10^{7}	2.6×10^{7}	2.6×10^{7}	2.9×10^{7}	4.1×10^{7}
CO	1.6×10^{8}	1.8×10^{19}	1.6×10^{8}	1.6×10^{9}	1.6×10^{9}	1.6×10^{9}	—	1.7×10^{9}	1.7×10^{9}	1.7×10^{9}	1.6×10^{8}	1.6×10^{8}	1.6×10^{8}	1.6×10^{8}
G2_circuit	1.0×10^{9}	1.2×10^{8}	9.9×10^{6}	6.4×10^{6}	6.4×10^{6}	6.4×10^{6}	6.6×10^{6}	6.7×10^{6}	7.8×10^{6}	8.2×10^{6}	6.4×10^{6}	6.4×10^{6}	6.8×10^{6}	9.0×10^{6}
Ga19As19H42	—	—	—	7.5×10^{8}	7.3×10^{8}	7.7×10^{8}	7.8×10^{8}	8.0×10^{8}	7.9×10^{8}	8.2×10^{8}	—	—	—	—
Si87H76	—	—	—	—	—	1.9×10^{9}	1.9×10^{9}	2.0×10^{9}	—	—	—	—	—	—
SiH4	6.8×10^{6}	5.8×10^{6}	5.8×10^{6}	3.7×10^{6}	3.4×10^{6}	3.7×10^{6}	3.9×10^{6}	3.5×10^{6}	3.9×10^{6}	4.0×10^{6}	3.7×10^{6}	4.0×10^{6}	5.3×10^{6}	7.4×10^{6}
apache1	6.5×10^{7}	4.4×10^{7}	1.3×10^{7}	1.0×10^{7}	9.9×10^{6}	1.0×10^{7}	1.0×10^{7}	9.7×10^{6}	1.3×10^{7}	1.3×10^{7}	1.0×10^{7}	1.0×10^{7}	9.5×10^{6}	1.1×10^{7}
apache2	—	—	1.8×10^{8}	1.3×10^{8}	1.2×10^{8}	1.3×10^{8}	1.3×10^{8}	1.4×10^{8}	1.5×10^{8}	1.7×10^{8}	1.4×10^{8}	—	—	—
auto	—	—	5.7×10^{8}	2.2×10^{8}	2.2×10^{8}	2.2×10^{8}	2.2×10^{8}	2.2×10^{8}	2.4×10^{8}	2.4×10^{8}	2.2×10^{8}	2.3×10^{8}	—	—
boyd2	2.7×10^{8}	2.8×10^{8}	8.1×10^{5}	8.0×10^{5}	8.9×10^{5}	8.9×10^{5}	8.9×10^{5}	8.9×10^{5}	1.6×10^{6}	1.8×10^{9}	8.0×10^{5}	8.0×10^{5}	8.0×10^{5}	8.0×10^{5}
c-55	—	—	4.6×10^{6}	3.5×10^{6}	3.2×10^{6}	3.2×10^{6}	3.4×10^{6}	3.7×10^{6}	3.8×10^{6}	4.5×10^{6}	3.2×10^{6}	3.3×10^{6}	5.1×10^{6}	7.6×10^{6}
c-70	3.0×10^{8}	1.1×10^{8}	4.0×10^{6}	3.1×10^{6}	3.1×10^{6}	3.1×10^{6}	3.1×10^{6}	3.0×10^{6}	4.6×10^{6}	3.7×10^{6}	2.9×10^{6}	3.0×10^{6}	3.8×10^{6}	5.1×10^{6}
ca-AstroPh	—	—	7.2×10^{6}	8.0×10^{6}	8.2×10^{6}	8.2×10^{6}	7.8×10^{6}	1.0×10^{7}	—	—	7.0×10^{6}	7.0×10^{6}	9.1×10^{6}	1.1×10^{7}
circuit_3	2.7×10^{4}	1.3×10^{6}	2.6×10^{4}	2.9×10^{4}	2.9×10^{4}	2.9×10^{4}	3.0×10^{4}	2.9×10^{4}	4.6×10^{4}	4.7×10^{4}	2.8×10^{4}	2.9×10^{4}	2.9×10^{4}	2.9×10^{4}
citationCiteseer	—	—	6.7×10^{8}	—	2.7×10^{8}	2.7×10^{8}	2.7×10^{8}	3.2×10^{8}	—	—	—	—	—	—
copter2	7.0×10^{8}	6.9×10^{7}	1.4×10^{7}	8.9×10^{6}	8.9×10^{6}	8.9×10^{6}	9.1×10^{6}	9.4×10^{6}	1.1×10^{7}	1.1×10^{7}	8.9×10^{6}	9.3×10^{6}	1.1×10^{7}	1.5×10^{7}
crystk03	1.4×10^{7}	1.4×10^{7}	1.3×10^{7}	9.2×10^{6}	9.2×10^{6}	9.2×10^{6}	9.2×10^{6}	9.2×10^{6}	1.0×10^{7}	1.0×10^{7}	9.2×10^{6}	9.2×10^{6}	9.2×10^{6}	9.6×10^{6}
delaunay_n20	—	—	4.0×10^{7}	3.4×10^{7}	3.3×10^{7}	3.3×10^{7}	3.4×10^{7}	3.4×10^{7}	4.2×10^{7}	4.3×10^{7}	3.3×10^{7}	3.3×10^{7}	3.4×10^{7}	3.8×10^{7}
dictionary28	7.9×10^{7}	1.8×10^{7}	6.3×10^{6}	4.1×10^{6}	4.1×10^{6}	4.1×10^{6}	4.3×10^{6}	4.3×10^{6}	4.8×10^{6}	4.8×10^{6}	4.1×10^{6}	4.0×10^{6}	4.6×10^{6}	5.9×10^{6}
ex10	9.1×10^{4}	7.0×10^{4}	4.7×10^{4}	5.7×10^{4}	5.7×10^{4}	5.7×10^{4}	5.8×10^{4}	5.8×10^{4}	7.0×10^{4}	7.5×10^{4}	5.7×10^{4}	5.9×10^{4}	6.1×10^{4}	5.6×10^{4}
gupta2	5.4×10^{8}	4.7×10^{8}	6.0×10^{6}	5.8×10^{6}	—	5.8×10^{6}	5.7×10^{6}	6.2×10^{6}	7.4×10^{6}	7.6×10^{6}	5.4×10^{8}	5.4×10^{8}	5.4×10^{8}	5.4×10^{8}
gupta3	5.4×10^{6}	1.3×10^{8}	5.4×10^{6}	1.0×10^{7}	—	1.0×10^{7}	1.0×10^{7}	8.6×10^{6}	1.0×10^{7}	9.9×10^{6}	5.4×10^{6}	5.4×10^{6}	5.4×10^{6}	5.4×10^{6}
lpl1	—	—	9.4×10^{5}	1.0×10^{6}	9.7×10^{5}	9.7×10^{5}	1.0×10^{6}	1.0×10^{6}	1.7×10^{6}	1.6×10^{6}	9.8×10^{5}	1.0×10^{6}	1.2×10^{6}	1.6×10^{6}
memplus	1.4×10^{8}	1.4×10^{5}	5.2×10^{4}	5.5×10^{4}	5.6×10^{4}	5.6×10^{4}	5.6×10^{4}	5.7×10^{4}	1.5×10^{5}	1.5×10^{5}	5.6×10^{4}	5.5×10^{4}	5.5×10^{4}	5.7×10^{4}
nasasrb	1.7×10^{7}	2.0×10^{7}	1.2×10^{7}	1.0×10^{7}	1.0×10^{7}	1.0×10^{7}	1.0×10^{7}	1.0×10^{7}	1.1×10^{7}	1.2×10^{7}	1.0×10^{7}	1.0×10^{7}	9.9×10^{6}	1.0×10^{7}
ncvxbqp1	—	—	4.2×10^{6}	1.9×10^{6}	1.9×10^{6}	1.9×10^{6}	1.9×10^{6}	1.9×10^{6}	2.2×10^{6}	2.3×10^{6}	1.9×10^{6}	1.9×10^{6}	2.0×10^{6}	2.7×10^{6}
parabolic_fem	—	2.2×10^{8}	3.6×10^{7}	2.5×10^{7}	2.5×10^{7}	2.5×10^{7}	2.5×10^{7}	2.5×10^{7}	2.9×10^{7}	2.9×10^{7}	2.5×10^{7}	2.5×10^{7}	2.6×10^{7}	3.1×10^{7}
rajat06	2.0×10^{6}	7.3×10^{5}	1.2×10^{5}	1.0×10^{5}	1.0×10^{5}	1.0×10^{5}	1.0×10^{5}	1.0×10^{5}	2.0×10^{5}	2.3×10^{5}	1.0×10^{5}	1.0×10^{5}	1.1×10^{5}	1.2×10^{5}
rajat10	7.4×10^{6}	3.3×10^{6}	4.0×10^{5}	3.4×10^{5}	3.4×10^{5}	3.4×10^{5}	3.4×10^{5}	3.4×10^{5}	6.3×10^{5}	6.6×10^{5}	3.4×10^{5}	3.4×10^{5}	3.5×10^{5}	3.6×10^{5}
rajat15	8.1×10^{6}	—	7.7×10^{5}	7.7×10^{5}	7.6×10^{5}	7.6×10^{5}	7.7×10^{5}	7.7×10^{5}	1.0×10^{6}	1.1×10^{6}	7.9×10^{5}	7.8×10^{5}	8.5×10^{5}	1.1×10^{6}
airpoll_conditional_st3	1.2×10^{7}	2.5×10^{7}	8.5×10^{6}	6.9×10^{6}	6.8×10^{6}	7.2×10^{6}	7.2×10^{6}	8.4×10^{6}	7.0×10^{6}	7.0×10^{6}	6.8×10^{6}	7.3×10^{6}	6.9×10^{6}	1.0×10^{7}
airpoll_prior_st3	1.2×10^{7}	9.0×10^{6}	8.4×10^{6}	6.8×10^{6}	6.8×10^{6}	7.1×10^{6}	7.1×10^{6}	8.3×10^{6}	7.1×10^{6}	6.8×10^{6}	6.8×10^{6}	7.1×10^{6}	6.8×10^{6}	9.9×10^{6}
cnt_cp2k	6.0×10^{6}	5.9×10^{6}	8.4×10^{6}	6.0×10^{6}	6.0×10^{6}	6.0×10^{6}	6.0×10^{6}	6.0×10^{6}	1.0×10^{7}	1.0×10^{7}	—	1.0×10^{7}	1.0×10^{7}	1.0×10^{7}
cnt_w90	3.5×10^{4}	3.5×10^{4}	3.5×10^{4}	4.3×10^{4}	5.2×10^{4}	5.3×10^{4}	5.4×10^{4}	5.0×10^{4}	3.5×10^{4}	5.2×10^{4}	5.2×10^{4}	5.3×10^{4}	4.6×10^{4}	3.5×10^{4}
kmc_potential_0	7.9×10^{8}	—	7.9×10^{8}	—	—	—	—	3.1×10^{8}	—	3.1×10^{8}	3.2×10^{8}	3.1×10^{8}	3.4×10^{8}	—
kmc_potential_1	—	—	—	—	—	—	—	—	—	1.8×10^{9}	1.9×10^{9}	1.9×10^{9}	2.0×10^{9}	—
qubit_fem_b4	3.8×10^{8}	3.2×10^{8}	3.8×10^{8}	1.2×10^{8}	1.1×10^{8}	—	—	1.1×10^{8}	—	1.1×10^{8}	1.1×10^{8}	1.1×10^{8}	1.2×10^{8}	1.1×10^{8}
sinw_w90	2.7×10^{6}	2.7×10^{6}	2.7×10^{6}	2.7×10^{6}	2.7×10^{6}	2.7×10^{6}	2.7×10^{6}	5.0×10^{6}	2.7×10^{6}	4.9×10^{6}	4.9×10^{6}	5.0×10^{6}	4.7×10^{6}	2.7×10^{6}

Table A.1.: Fill-in (number of nonzeros after factorization) for each matrix and reordering algorithm.

Matrix	RCM	AMD	METIS	NDCustom	ParMETIS-2	ParMETIS-4	ParMETIS-8	SCOTCH	PT-SCOTCH	db-2	db-4	db-8	db-16
144	0.061	0.271	2.112	3.964	4.053	4.548	3.372	2.923	3.635	52.075	78.292	102.635	85.395
3Dspectralwave	0.746	0.0	19.562	0.0	39.765	34.463	30.827	35.659	27.972	0.0	0.0	0.0	0.0
598a	0.061	0.282	1.614	2.668	3.754	3.420	3.308	2.712	2.854	42.707	37.654	48.547	60.457
CO	0.144	0.0	4.985	86.865	12.658	11.394	10.552	11.558	9.062	0.0	0.0	0.0	0.0
G2_circuit	0.033	0.141	1.106	1.607	2.044	1.795	1.761	1.703	1.841	14.571	21.817	22.723	23.600
Ga19As19H42	0.109	0.0	3.158	101.233	11.712	11.782	10.504	10.647	9.527	0.0	0.0	0.0	0.0
Si87H76	0.208	0.0	0.0	0.0	16.080	15.123	13.743	13.481	12.879	0.0	0.0	0.0	0.0
SiH4	0.005	0.046	0.090	0.544	0.801	0.978	1.059	0.664	1.002	5.807	6.400	8.067	10.537
apache1	0.035	0.094	0.750	1.231	1.519	1.407	1.416	1.482	1.535	12.918	21.983	30.059	22.131
apache2	0.142	0.840	5.206	11.462	9.348	7.725	6.123	6.535	6.231	113.364	0.0	0.0	0.0
auto	0.243	1.564	5.927	13.647	11.815	10.773	9.497	7.134	8.113	212.413	273.232	0.0	0.0
boyd2	0.074	0.134	1.364	62.858	4.383	3.674	3.291	10.078	6.315	18.900	21.477	21.597	36.917
c-55	0.017	0.066	0.295	1.529	1.562	1.592	1.849	1.399	1.720	17.803	36.937	48.612	80.473
c-70	0.031	0.094	0.766	1.627	2.068	2.268	2.307	1.443	1.984	18.863	26.485	36.458	48.367
ca-AstroPh	0.013	0.087	0.257	1.320	1.396	1.587	2.018	1.178	1.331	13.562	19.613	21.744	28.675
circuit_3	0.006	0.008	0.064	0.087	0.575	0.540	0.627	0.454	0.718	3.602	3.406	3.410	3.829
citationCiteseer	0.099	1.542	3.264	29.040	9.516	8.943	7.717	7.221	5.452	252.821	0.0	0.0	0.0
copter2	0.023	0.151	0.733	1.269	1.924	1.819	1.861	1.547	1.734	14.522	30.263	30.062	27.043
crystk03	0.025	0.084	0.210	0.690	2.424	2.507	2.788	1.644	2.396	16.430	15.065	15.106	17.250
delaunay_n20	0.257	1.370	6.845	11.794	12.832	10.401	9.045	7.237	7.808	127.681	214.854	270.887	252.652
dictionary28	0.013	0.059	0.343	0.729	1.091	1.164	1.269	1.258	1.330	9.888	8.965	7.783	8.655
ex10	0.006	0.012	0.030	0.048	0.533	0.566	0.584	0.254	0.639	3.520	3.189	3.583	3.347
gupta2	0.065	2.075	0.900	0.0	7.038	8.940	7.081	6.420	5.357	0.0	0.0	0.0	0.0
gupta3	0.116	0.688	0.786	0.0	10.923	11.779	11.283	7.724	7.261	0.0	0.0	0.0	0.0
lpl1	0.011	0.080	0.373	1.668	1.149	1.206	1.481	1.377	1.413	6.590	8.509	8.016	11.014
memplus	0.006	0.032	0.073	0.183	0.674	0.750	0.832	0.424	0.936	4.374	5.776	6.287	8.373
nasasrb	0.064	0.169	0.613	1.539	3.587	3.526	2.807	2.406	3.199	20.019	20.685	20.413	21.757
ncvxbqp1	0.017	0.068	0.420	0.604	1.238	1.154	1.169	1.134	1.206	8.660	17.101	11.923	11.470
parabolic_fem	0.088	0.348	2.937	5.803	6.332	5.607	5.099	4.100	4.370	44.500	63.501	61.983	95.454
rajat06	0.004	0.009	0.061	0.078	0.532	0.555	0.607	0.408	0.779	2.802	3.827	4.136	4.066
rajat10	0.018	0.019	0.148	0.204	0.730	0.727	0.767	0.631	0.925	4.317	4.326	4.974	5.796
rajat15	0.019	0.078	0.399	1.008	1.330	1.268	1.355	1.495	1.486	9.842	10.911	14.023	17.835
airpoll_conditional_st3	0.025	0.085	0.318	12.282	2.324	2.515	2.203	2.252	2.203	53.457	43.843	45.646	49.021
airpoll_prior_st3	0.017	0.084	0.150	1.830	2.327	2.544	2.229	1.309	2.229	37.342	35.457	35.548	36.613
cnt_cp2k	0.064	0.277	0.717	—	6.220	7.732	5.158	4.865	5.158	0.0	0.0	0.0	0.0
cnt_w90	0.005	0.010	0.007	0.160	0.717	0.553	0.730	0.109	0.730	2.899	10.420	3.349	2.784
kmc_potential_0	0.332	1.094	5.709	61.167	13.940	13.016	10.575	11.459	10.575	0.0	0.0	0.0	0.0
kmc_potential_1	1.515	0.0	0.0	317.549	55.518	49.505	34.982	37.262	34.982	0.0	0.0	0.0	0.0
qubit_fem_b4	0.068	0.453	2.193	22.243	4.611	4.305	4.278	4.672	4.278	237.962	72.351	0.0	0.0
sinw_w90	0.097	0.235	0.269	5.145	4.872	5.167	3.668	2.223	3.668	0.0	0.0	0.0	0.0

Table A.2.: Reordering time (seconds) for each matrix and reordering algorithm.

Matrix	RCM	AMD	METIS	NDCustom	ParMETIS-2	ParMETIS-4	ParMETIS-8	SCOTCH	PT-SCOTCH	db-2	db-4	db-8	db-16
144	3357	3357	55668	149388	151504	151220	150680	82500	85588	12	12	12	12
3Dspectralwave	1150k	0	1121k	0	2750k	2750k	2750k	2014k	2011k	0	0	0	0
598a	900	536	41088	127660	130220	129460	128680	80972	81096	292	412	344	616
CO	11978	0	11978	608508	580512	520376	609568	342212	342204	0	0	0	0
G2_circuit	1135	1135	4864	13312	16072	15480	14840	9776	10332	48	12	12	64
Ga19As19H42	151000	0	125920	643008	679272	678784	643800	445332	445008	0	0	0	0
Si87H76	159656	0	0	0	824620	823872	781728	579816	581828	0	0	0	0
SiH4	269	269	269	4	4	4	4	4	4	12	12	12	12
apache1	847	847	847	4	4	4	4	4	4	12	12	12	12
apache2	7528	7528	7528	373028	375932	337520	374576	246656	249608	63816	0	0	0
auto	10358	10358	10358	523376	576724	525164	524616	315020	313500	53720	12	0	0
boyd2	2344	2344	4416	98424	101928	100804	100392	102548	103336	108	12	104	12
c-55	630	630	630	4312	4556	4668	4728	4	4	64	12	12	12
c-70	1030	1030	1030	4	4	4	4	4	4	12	12	12	12
ca-AstroPh	619	619	619	13620	13672	13884	13404	4128	3384	12	12	12	12
circuit_3	69	69	69	4	4	4	4	4	4	12	12	12	12
citationCiteseer	3615	3615	35420	154172	156948	155652	155100	101168	101444	12	0	0	0
copter2	1187	1187	1187	4	4	4	4	4	4	12	12	12	12
crystk03	2736	2736	2736	100080	101108	101100	114396	52984	52928	1652	1064	1104	2764
delaunay_n20	9830	9830	1528	637464	665980	640752	639516	490916	442864	75320	136	81396	296
dictionary28	278	278	278	5728	8740	7824	7040	4668	4968	16	16	16	12
ex10	86	86	86	86	4	4	4	4	4	12	12	12	12
gupta2	9992	6638	6638	0	280616	247160	313728	171140	137372	0	0	0	0
gupta3	173344	145608	139524	0	712232	712240	675556	417288	417288	0	0	0	0
lpl1	513	513	513	4	4	4	4	4	4	12	12	12	12
memplus	158	158	158	4	4	4	4	4	4	12	12	12	12
nasasrb	4183	4183	4183	124060	123856	123856	123776	63288	63748	12	12	12	12
ncvxbqp1	547	547	547	4	4	4	4	4	4	12	12	12	12
parabolic_fem	5742	5742	19036	247344	249628	249176	277156	164000	169548	716	300	27156	304
rajat06	73	73	73	4	4	4	4	4	4	12	12	12	12
rajat10	204	204	204	4	4	4	4	4	4	12	12	12	12
rajat15	693	693	693	4	4	4	4	4	4	12	12	12	12
airpoll_conditional_st3	1904	1904	1904	69680	69920	69924	31688	31820	31688	368	268	644	816
airpoll_prior_st3	1884	1884	1884	63548	63796	63740	25948	26368	25948	12	460	280	28
cnt_cp2k	30944	9616	9616	0	383284	432120	236364	188276	236364	0	0	0	0
cnt_w90	112	112	112	2724	3240	2984	248	4	248	368	1768	1128	1588
kmc_potential_0	144440	78184	109184	899528	901560	938900	668216	627736	668216	0	0	0	0
kmc_potential_1	921224	0	0	3861296	3863608	3862000	2778032	2773948	2778032	0	0	0	0
qubit_fem_b4	43616	4	24760	193464	193972	233052	109816	109204	109816	35500	76532	0	0
sinw_w90	76128	46336	48448	417968	417920	430000	249648	249640	249648	0	0	0	0

Table A.3.: Maximum memory usage (KB) during reordering for each matrix and algorithm.

Matrix	RCM	AMD	METIS	NDCustom	ParMETIS-2	ParMETIS-4	ParMETIS-8	SCOTCH	PT-SCOTCH	db-2	db-4	db-8	db-16
144	2350	2350	27834	24469	40703	58832	48525	12380	16450	12.0	12.0	12.0	12.0
3Dspectralwave	461793	0	460086	0	1120933	1317370	1470425	425597	548462	0.0	0.0	0.0	0.0
598a	472	211	13696	22727	46393	50232	49445	16556	16260	292	411	305	615
CO	8385	0	8385	48144	175532	155282	219679	50329	58432	0.0	0.0	0.0	0.0
G2_circuit	795	795	2432	1784	3398	3839	3803	335	335	48	12	12	64
Ga19As19H42	58637	0	60509	19684	260046	265948	245076	87241	98637	0.0	0.0	0.0	0.0
Si87H76	60738	0	0	0	280158	300024	298703	121061	123001	0.0	0.0	0.0	0.0
SiH4	188	188	188	3	3	3	3	3	3	12	12	12	12
apache1	593	593	593	3	3	3	3	3	3	12	12	12	12
apache2	5270	5270	5270	26732	91929	94912	125461	34939	37490	70	0.0	0.0	0.0
auto	7251	7251	7251	54253	198083	189256	206590	67046	71388	31	12	0.0	0.0
boyd2	1641	1641	2376	3267	24068	19810	23174	5428	6840	108	12	104	12
c-55	441	441	441	254	680	631	537	3	3	64	12	12	12
c-70	721	721	721	3	3	3	3	3	3	12	12	12	12
ca-AstroPh	433	433	433	1865	2634	3039	2391	1144	401	12	12	12	12
circuit_3	48	48	48	3	3	3	3	3	3	12	12	12	12
citationCiteseer	2530	2530	11807	9830	34397	34500	29824	7963	10522	12	0.0	0.0	0.0
copter2	831	831	831	3	3	3	3	3	3	12	12	12	12
crystk03	1915	1915	1915	50792	42837	42193	51024	18628	11867	1520	15	1100	294
delaunay_n20	6881	6881	382	59146	199813	207967	242155	130707	102073	444	136	202	296
dictionary28	195	195	195	1460	2297	2268	2000	754	984	16	16	16	12
ex10	60	60	60	60	3	3	3	3	3	12	12	12	12
gupta2	4996	4647	4647	0	68475	98880	102083	24630	22404	0.0	0.0	0.0	0.0
gupta3	58665	86992	61466	0	272550	260201	231491	115501	109466	0.0	0.0	0.0	0.0
lpl1	359	359	359	4	3	3	3	3	3	12	12	12	12
memplus	110	110	110	3	3	3	3	3	3	12	12	12	12
nasasrb	2928	2928	2928	38015	50166	51248	38556	16725	12230	12	12	12	12
ncvxbqp1	383	383	383	3	3	3	3	3	3	12	12	12	12
parabolic_fem	4019	4019	9518	31722	64371	72374	108678	27836	28283	587	300	34	304
rajat06	51	51	51	2	3	3	3	3	4	12	12	12	12
rajat10	143	143	143	3	3	3	3	3	3	12	12	12	12
rajat15	485	485	485	3	3	3	3	3	3	12	12	12	12
airpoll_conditional_st3	1333	1333	1333	6057	24380	22278	6247	6186	6247	368	252	643	799
airpoll_prior_st3	1319	1319	1319	28778	22287	20688	4871	9500	4871	0	443	264	28
cnt_cp2k	15472	6731	6731	0	119047	145990	47787	38493	47787	0	0	0	0
cnt_w90	78	78	78	810	441	487	231	1	231	361	195	44	167
kmc_potential_0	43898	32282	63399	73563	321702	392351	160563	149829	160563	0	0	0	0
kmc_potential_1	438089	0	0	279053	1605689	1848255	869721	790627	869721	0	0	0	0
qubit_fem_b4	21808	2	12380	14494	66102	90042	19132	17100	19132	375	121	0	0
sinw_w90	38064	15447	16151	144526	174394	171231	65498	122032	65498	0	0	0	0

Table A.4.: Average memory usage (KB) during reordering for each matrix and algorithm.

Matrix	RCM	AMD	METIS	NDCustom	ParMETIS-2	ParMETIS-4	ParMETIS-8	SCOTCH	PT-SCOTCH	db-2	db-4	db-8	db-16
144	380	56	47	86	33	30	31	265	215	49	79	66	85
3Dspectralwave	569	830	279	830	244	254	258	966	—	830	830	830	830
598a	398	46	57	62	30	26	27	182	188	52	52	64	113
CO	982	—	160	839	—	—	—	1103	1070	—	—	—	—
G2_circuit	212	11	12	101	100	99	103	93	54	11	33	100	100
Ga19As19H42	—	—	639	560	—	—	—	—	1009	—	—	—	—
Si87H76	1012	—	—	—	—	—	—	1039	929	—	—	—	—
SiH4	329	382	130	397	220	192	165	194	399	173	468	609	798
apache1	206	4	12	12	106	120	110	22	35	19	25	13	18
apache2	357	2	11	13	305	318	332	131	85	17	603	603	603
auto	622	58	89	171	41	39	37	351	329	82	102	204	204
boyd2	5	4	3	2	6	10	9	3	5	3	3	3	3
c-55	10	23	37	26	31	30	26	33	25	29	27	23	19
c-70	10	19	42	36	22	32	25	23	27	33	29	29	26
ca-AstroPh	184	105	112	124	52	56	49	183	246	113	116	115	105
circuit_3	19	27	12	14	15	12	13	17	17	12	13	12	11
citationCiteseer	76	40	47	52	30	36	30	78	133	48	32	32	32
copter2	404	60	53	57	41	42	43	148	91	65	76	79	82
crystk03	719	251	126	125	212	273	164	290	328	173	179	203	218
delaunay_n20	—	24	26	26	36	42	37	—	—	29	25	24	25
dictionary28	67	35	30	35	24	30	33	70	46	37	29	30	36
ex10	354	92	55	67	53	47	61	49	59	73	59	79	62
gupta2	83	39	59	26	87	81	99	55	54	26	26	26	26
gupta3	531	329	225	301	953	788	470	572	668	301	301	301	301
lpl1	33	20	29	21	21	21	22	23	21	29	20	25	21
memplus	34	33	48	40	25	14	19	45	46	47	43	34	35
nasasrb	—	447	166	135	152	125	169	327	487	171	236	280	324
ncvxbqp1	118	18	22	22	16	14	15	95	95	23	21	21	27
parabolic_fem	—	31	22	24	17	16	17	964	743	23	23	26	25
rajat06	81	5	7	6	31	29	24	10	10	7	6	6	7
rajat10	135	5	6	6	27	35	33	10	10	7	6	8	8
rajat15	77	81	62	66	31	33	35	92	99	60	56	59	58
airpoll_conditional_st3	360	400	330	422	243	291	817	1096	817	659	690	473	514
airpoll_prior_st3	428	452	390	358	223	235	775	806	775	676	611	517	760
cnt_cp2k	—	—	1609	—	—	—	—	—	—	—	—	—	—
cnt_w90	767	735	95	95	111	190	223	767	223	95	95	95	95
kmc_potential_0	—	232	114	237	202	201	427	451	427	555	555	555	555
kmc_potential_1	—	571	571	287	383	332	810	706	810	571	571	571	571
qubit_fem_b4	248	116	45	60	82	75	140	104	140	98	80	225	225
sinw_w90	—	—	910	908	—	—	910	961	910	—	—	—	—

Table A.5.: Elimination tree depth for each matrix and reordering algorithm.

Appendix B

Task Description

List of Figures

List of Tables

List of Algorithms

Bibliography

[1] J. Scott and M. Tůma, "An Introduction to Sparse Matrices," in *Algorithms for Sparse Linear Systems*, J. Scott and M. Tůma, Eds. Cham: Springer International Publishing, 2023, pp. 1–5. [Online]. Available: https://doi.org/10.1007/978-3-031-25820-6_1

[2] H. Schaeffer, R. Caflisch, C. D. Hauck, and S. Osher, "Sparse dynamics for partial differential equations," *Proceedings of the National Academy of Sciences*, vol. 110, no. 17, pp. 6634–6639, Apr. 2013, publisher: Proceedings of the National Academy of Sciences. [Online]. Available: https://www.pnas.org/doi/10.1073/pnas.1302752110

[3] J. R. Gilbert and R. E. Tarjan, "The analysis of a nested dissection algorithm," *Numerische Mathematik*, vol. 50, no. 4, pp. 377–404, Jul. 1986. [Online]. Available: https://doi.org/10.1007/BF01396660

[4] M. Yannakakis, "Computing the Minimum Fill-In is NP-Complete," *SIAM Journal on Algebraic Discrete Methods*, vol. 2, no. 1, pp. 77–79, Mar. 1981, publisher: Society for Industrial and Applied Mathematics. [Online]. Available: https://epubs.siam.org/doi/10.1137/0602010

[5] E. Cuthill and J. McKee, "Reducing the bandwidth of sparse symmetric matrices," in *Proceedings of the 1969 24th National Conference*, ser. ACM '69. New York, NY, USA: ACM, 1969, pp. 157–172.

[6] A. George and J. W. H. Liu, "Computer solution of large sparse positive definite systems," *Prentice-Hall Series in Computational Mathematics*, 1981.

[7] W. F. Tinney and J. W. Walker, "Direct solutions of sparse network equations by optimally ordered triangular factorization," *Proceedings of the IEEE*, vol. 55, no. 11, pp. 1801–1809, 1967.

[8] J. W. H. Liu, "Modification of the minimum-degree algorithm by multiple elimination," *ACM Transactions on Mathematical Software*, vol. 11, no. 2, pp. 141–153, 1985.

[9] P. R. Amestoy, T. A. Davis, and I. S. Duff, "An approximate minimum degree ordering algorithm," *SIAM Journal on Matrix Analysis and Applications*, vol. 17, no. 4, pp. 886–905, 1996.

[10] R. J. Lipton, D. J. Rose, and R. E. Tarjan, "Generalized Nested Dissection," *SIAM Journal on Numerical Analysis*, vol. 16, no. 2, pp. 346–358, Apr. 1979, publisher: Society for Industrial and Applied Mathematics. [Online]. Available: https://epubs.siam.org/doi/10.1137/0716027

[11] A. George, "Nested Dissection of a Regular Finite Element Mesh," *SIAM Journal on Numerical Analysis*, vol. 10, no. 2, pp. 345–363, Apr. 1973, publisher: Society for Industrial and Applied Mathematics. [Online]. Available: https://epubs.siam.org/doi/10.1137/0710032

[12] U. V. Çatalyürek, C. Aykanat, and E. Kayaaslan, "Hypergraph Partitioning-Based Fill-Reducing Ordering for Symmetric Matrices," *SIAM Journal on Scientific Computing*, vol. 33, no. 4, pp. 1996–2023, Jan. 2011, publisher: Society for Industrial and Applied Mathematics. [Online]. Available: https://epubs.siam.org/doi/10.1137/090757575

[13] A. Dasgupta and P. Kumar, "Alpha Elimination: Using Deep Reinforcement Learning to Reduce Fill-In During Sparse Matrix Decomposition," in *Machine Learning and Knowledge Discovery in Databases: Research Track: European Conference, ECML PKDD 2023, Turin, Italy, September 18–22, 2023, Proceedings, Part IV*. Berlin, Heidelberg: Springer-Verlag, Sep. 2023, pp. 472–488. [Online]. Available: https://doi.org/10.1007/978-3-031-43421-1_28

[14] O. Selvitopi, S. Acer, M. Manguoğlu, and C. Aykanat, "The Effect of Various Sparsity Structures on Parallelism and Algorithms to Reveal Those Structures," in *Parallel Algorithms in Computational Science and Engineering*, A. Grama and A. H. Sameh, Eds. Cham: Springer International Publishing, 2020, pp. 35–62. [Online]. Available: https://doi.org/10.1007/978-3-030-43736-7_2

[15] D. Merrill, "Scalable GPU Graph Traversal."

[16] P. Kaleta, "kaletap/bfs-cuda-gpu," May 2025, original-date: 2019-11-14T12:55:50Z. [Online]. Available: https://github.com/kaletap/bfs-cuda-gpu

[17] C. Yuan, "Fast Sparse Matrix Reordering on GPU for Cholesky Based Solvers."

[18] M. S. Gilbert, K. Madduri, E. G. Boman, and S. Rajamanickam, "Jet: Multilevel Graph Partitioning on Graphics Processing Units," *SIAM Journal on Scientific Computing*, vol. 46, no. 5, pp. B700–B724, Oct. 2024, publisher: Society for Industrial and Applied Mathematics. [Online]. Available: https://epubs.siam.org/doi/10.1137/23M1559129

[19] H. Kaeslin, *Digital Integrated Circuit Design: From VLSI Architectures to CMOS Fabrication*. Cambridge University Press, Apr. 2008.

[20] D. Hankerson, S. Vanstone, and A. Menezes, *Guide to Elliptic Curve Cryptography*, ser. Springer Professional Computing. Springer, 2004.

[21] NIST, *Advanced Encryption Standard (AES) (FIPS PUB 197)*, National Institute of Standards and Technology, Nov. 2001.

[22] P. Rogaway, M. Bellare, J. Black, and T. Krovetz, "OCB: A block-cipher mode of operation for efficient authenticated encryption," in *ACM Conference on Computer and Communications Security*, 2001, pp. 196–205.

[23] Xilinx. (2011, Nov.) Virtex-6 FPGA Configuration User Guide. UG360 (v3.4). [Online]. Available: http://www.xilinx.com/support/documentation/user_guides/ug360.pdf

[24] ——. (2011, Oct.) 7 Series FPGAs Configuration User Guide. UG470 (v1.2). [Online]. Available: http://www.xilinx.com/support/documentation/user_guides/ug470_7Series_Config.pdf

[25] Wikipedia, "Isaac Newton," accessed October 1, 2012. [Online]. Available: http://en.wikipedia.org/w/index.php?title=Isaac_Newton&oldid=514997436

[26] Y.-H. Chang, A. Buluç, and J. Demmel, "Parallelizing the approximate minimum degree ordering algorithm: Strategies and evaluation," 2025. [Online]. Available: https://arxiv.org/abs/2504.17097

[27] P. R. Amestoy, T. A. Davis, and I. S. Duff, "Algorithm 837: AMD, an approximate minimum degree ordering algorithm," *ACM Transactions on Mathematical Software*, vol. 30, no. 3, pp. 381–388, Sep. 2004.